Sea Surface Temperature proxy comparison for the Pliocene North Sea

Master's thesis

Christine Boschman

Supervisors:

Emily Dearing Crampton-Flood and Francien Peterse

Utrecht University

October 2016

Abstract

The Pliocene (5.3 – 2.6 Ma) is seen as a good analogue for the climate of the near future, due to slightly higher global temperatures (i.e. 2-3 °C) and similar atmospheric CO_2 concentrations (400 ppm) compared to the present. However, reliable data are needed to validate models that make projections of future climate. In this study, we have used sediments from a core in the coastal North Sea to test and compare three sea surface temperature (SST) proxies based on biomarkers: i.e. $U^{K'}_{37}$, TEX_{86}^{H} and LDI, on their ability to reconstruct SSTs of the Pliocene North Sea. The SSTs are compared with the continental mean air temperature record of the same site produced using biomarkers (branched GDGTs). The influence of sea level changes and terrestrial input are also investigated. The SST proxy comparison demonstrates that the $U^{K'}_{37}$ and LDI proxies respond to the same driver, i.e. temperature, but to a different extent, probably due to different production seasons of the biomarkers used in the proxies. The TEX_{86}^{H} proxy shows trends not consistent with the other two SST proxies, and is therefore assumed not reliable in this setting. Large fluctuations in SSTs are seen, most likely caused by changes in the configuration of the North Atlantic current. Finally, comparison of the marine and terrestrial climates shows that they are decoupled. The mechanism for this decoupling could be a result of regional ocean currents influencing marine climate, while the terrestrial climate largely follows global climate fluctuations.

Table of contents

Abstract 2
Table of contents 3
1. Introduction 4
2. Methods 6
2.1. Materials 6
2.2. Age model 6
2.3. Extraction and lipid analysis 8
2.4. Proxy calculations 8
2.5. Cyclicity 9
2.6. Alkenone stable carbon isotope analysis 9
2.7. Bulk elemental analysis 9
2.8. Alkenone pCO_2 estimates 10
3. Results 10
3.1. Age model and lithology 10
3.2. Sea surface temperature proxy comparison 11
3.3. Terrestrial input 12
4. Discussion 13
4.1. SST proxy comparison 13
4.1.1. SST proxy comparison; differences in absolute values 13
4.1.2. SST proxy comparison; differences in trends 14
4.2. Large fluctuations in SSTs; comparison with two North Atlantic SST records 14
4.3. Cyclicity in SST fluctuations 18
4.4. Comparison of the SST records with terrestrial climate and depositional environment 23
4.4.1. The Mid-Pliocene Warm Period 27
4.5. The alkenone pCO_2 proxy 29
5. Conclusions 30
Acknowledgements 31
References 31

1. Introduction

The Pliocene (5.3 – 2.6 million years ago (Ma)) is the epoch that directly preceded the onset of Northern Hemisphere Glaciations (NHG) (Bartoli et al., 2005, Naafs et al., 2010). Whereas Pleistocene temperatures show large fluctuations between glacials and interglacials, the relatively ice-free Pliocene is generally believed to possess a more stable climate (Lisiecki & Raymo, 2005). Atmospheric CO_2 concentrations of the Pliocene were similar to present values (400 ppm; Pagani et al., 2010) and temperatures were a few degrees higher than present (2 -3 °C; Dowsett, 2007, Haywood et al., 2009). As global temperatures lag atmospheric CO_2 level changes, a general temperature rise consisting of a few degrees is expected for the near future (Pagani et al., 2010, Martinez-Boti et al., 2015). Therefore, the Pliocene is seen as a good analogue for the climate of the near future. The Mid-Pliocene Warm Period (MPWP, 3.3 – 3.0 Ma) is especially studied to provide insight in future climate, as it is believed to resemble current climate once equilibrium is achieved.

The North Atlantic is especially relevant for global climate, as the ocean currents can influence glaciations in the Northern Hemisphere. Therefore, both the currents and the climate operating in the North Atlantic have major impacts on climate fluctuations (Dowsett et al., 2009). The North Sea, in particular, presents an opportunity to study both the Atlantic system and the terrestrial climate of Western Europe. Currents originating in the Atlantic are in contact with the North Sea, and sediments from the continent are deposited and stored in the North Sea basin. The past conditions of the North Atlantic Ocean and North Sea can be studied through Sea Surface Temperature (SST) reconstructions, a general indication of climate. Terrestrial climate, on the other hand, can be studied by Mean Air Temperature (MAT) reconstructions. There are currently two SST records of the North Atlantic based on alkenone paleothermometry (Lawrence et al., 2009, Naafs et al., 2010). Both records show large variations (~6 °C) over the Pliocene, which is remarkable, as Pliocene climate was considered to be relatively stable. Hardly any Pliocene records are available where both marine and terrestrial climate is reconstructed. Comparing the marine and terrestrial climate of the Pliocene would improve the understanding of the influence of the marine environment (e.g. ocean currents) on the terrestrial climate in a warmer world, and could therefore improve future climate predictions.

There are currently three marine organic geochemical temperature proxies available. The first, widely used proxy, is the $U^{K'}_{37}$ index. It is based on the relative abundance of C_{37-2} and C_{37-3} alkenones, whereby 37 refers to the number of carbon atoms and 2 and 3 refer to the degree of unsaturation (Fig. 1). Alkenones are produced by haptophyte algae, residing near the surface of the ocean (Prahl and Wakeham, 1987, Müller et al., 1998). The relative abundances of the C_{37-2} and C_{37-3} alkenones (i.e. the $U^{K'}_{37}$ index) is found to be related to SST. Based on core top measurements, a calibration is made to relate the $U^{K'}_{37}$ index to annual mean SSTs (Prahl and Wakeham, 1987, Müller et al., 1998). The second organic proxy for SST is the TEX_{86} index, also regularly used for climate reconstructions. The TEX_{86} index is based on glycerol dialkyl glycerol tetraethers (GDGTs, Fig. 2), which are membrane lipids produced by marine Thaumarchaeota, containing varying numbers of cyclopentane moieties (Schouten et al., 2002, 2013). TEX_{86} indices are strongly correlated (R^2 = 0.87) with annual mean SST in a global core top data set (Kim et al., 2008, 2010). Recently, a third organic proxy for SST was developed, the Long chain Diol Index (LDI; Rampen et al., 2012). The LDI reflects the ratio of the C_{30} 1,15 diol relative to the C_{28} 1,13, C_{30} 1,13 and C_{30} 1,15 diols (Fig. 3). The LDI also shows a strong correlation with annual mean SST in globally distributed surface sediments (Rampen et al., 2012). The biological source of long-chain diols in marine sediments is still uncertain (Versteegh et al., 1997,

Rampen et al., 2012). To date, the LDI has scarcely been applied in paleo studies (Naafs et al., 2012, Rodgrigo-Gámiz et al., 2014, 2015).

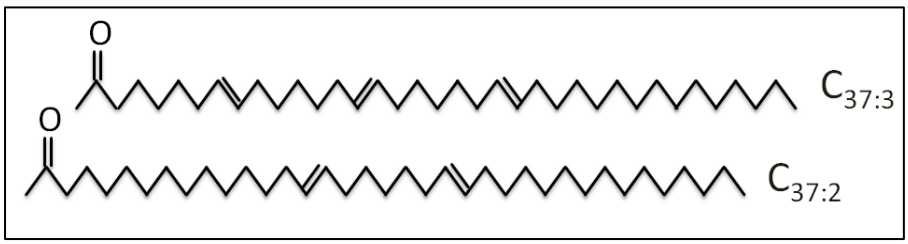

Figure 1. Structures of alkenones used for the $U^{K'}_{37}$ proxy.

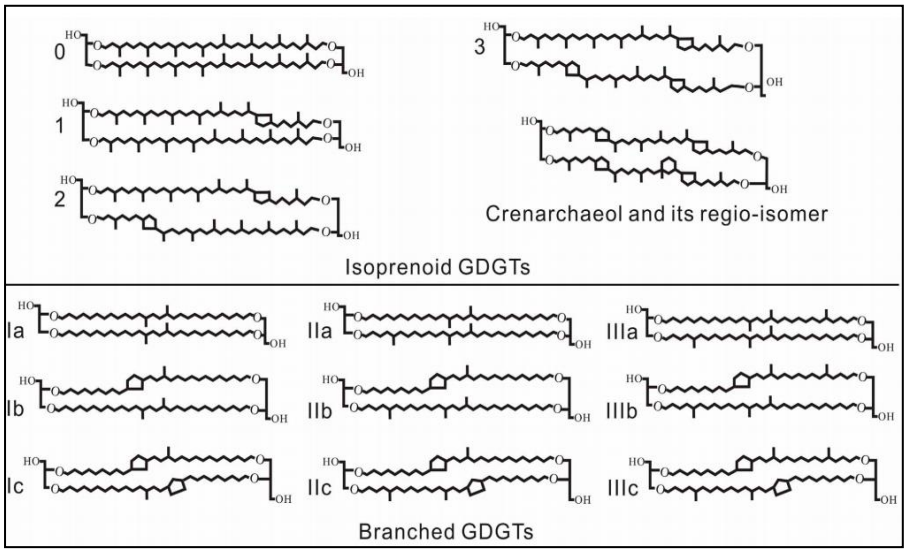

Figure 2. Structures of GDGTs used for the TEX_{86} proxy and the BIT index. From Jia et al., 2013.

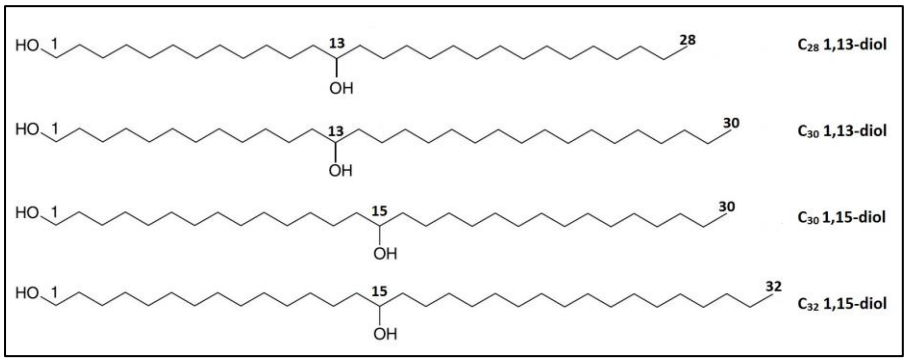

Figure 3. Structures of long chain diols used for the LDI and the %C32 proxies.

All three proxies demonstrate strong relationships with SST, however, as with all proxies for the past they possess some degree of uncertainty. Firstly, the $U^{K'}_{37}$ index may be affected by variations in nutrient concentrations, light limitation, and diagenesis (Hoefs et al., 1998, Gong and Hollander, 1999, Prahl et al., 2003, Rontani et al., 2013). Secondly, the TEX_{86} index can also be affected by diagenesis, although to a smaller extent than the $U^{K'}_{37}$ index (Schouten et al., 2013, Kim et al., 2009). The TEX_{86} index is also influenced by high terrestrial input. Thirdly, the effect of degradation and nutrient limitation on the LDI is not yet known (Rodrigo-Gámiz et al., 2015). Comparing results from the three proxies, that is, investigating the differences in their results and exploring the possible mechanisms resulting in those differences, might improve their reliability. Combining records of the three organic proxies will strengthen confidence in reconstructed SSTs of the Pliocene.

In this thesis, I will investigate the sea surface temperatures of the North Sea during the Pliocene by applying three independent SST proxies on the same sediment samples from the Hank Core. Hank is currently located onshore the Netherlands, but during the Pliocene this area was part of the North Sea (Fig. 1). The lithology of the core is composed of mainly sand, and biostratigraphy has demonstrated that it covers the time period from the Early Pliocene until present. The focus of this thesis is on the lower part (404-178m), containing Pliocene sediments. The reliability of the three SST records will be assessed by comparing the proxy records with each other and the literature.
To further interpret the SST signal and to place the SST records in a broader perspective, I aim to identify the astronomical forcing of SST variations. In addition, I will compare the SSTs with a MAT record for NW Europe derived from soil bacterial membrane lipids archived in the same core (Dearing Crampton-Flood et al., in prep), and assess the influence of sea level changes and terrestrial input on the SST records using the BIT index (branched over isoprenoid tetraether index, a GDGT based proxy for soil input (Hopmans et al., 2004)) and %C32 diols (a long chain diol based proxy for riverine organic matter input (Lattaud et al., 2016)). Finally, an attempt to reconstruct the atmospheric CO_2 concentrations during the Pliocene will be made to determine the implications of ongoing CO_2 rise on North Sea SSTs.

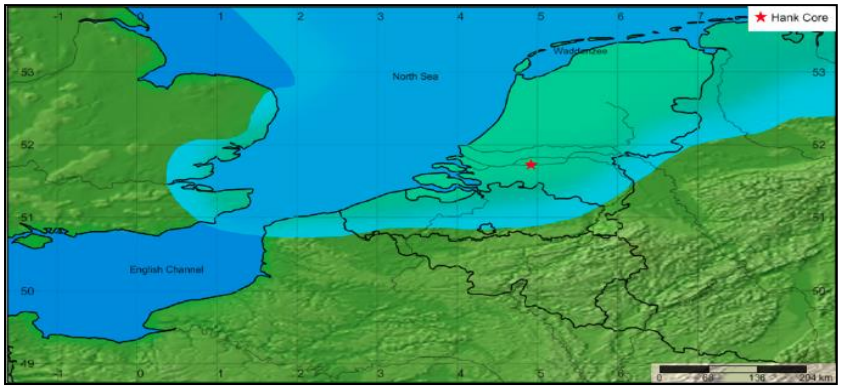

Figure 4. Location of the Hank Core and reconstructed paleo coastline of the Pliocene North Sea (Kuhlmann et al., 2006, Huuse et al., 2001, Ziegler, 1990).

2. Materials and methods

2.1. Materials

The Hank Core (Fig. 4) is located in a shallow marine environment. The Pliocene North Sea was a progradational delta system with a thick sedimentary infill (Kuhlmann et al., 2004). The Hank Core was drilled by the Geological Survey of the Netherlands using the air lift drilling method. Consequences of this method are a maximum sample resolution of one meter and an inaccuracy of one meter for each sample depth. 130 samples were taken every meter in the depth interval 178-404m. The main lithology is sand (Fig. 6). Some clay and loam is found, mainly in the lower part of the core, and some sandy shells are found in the upper part of the core.

2.2. Age model

The age model of the Hank Core is based on biostratigraphy (Dearing Crampton-Flood et al., in prep). Ages are based on last occurrence data (LODs) of dinoflagellates in the North Sea and North Atlantic

regions (Table 1, Fig. 5). The Hank Core includes the entire Pliocene (5.3 – 2.6 Ma, Zanclean and Piacenzian) and a part of the Gelasian (2.6 – 1.8 Ma, early Pleistocene). The distribution of tie-points indicates an increasing sedimentation rate over time (Fig. 5) but the coastal location also suggest sedimentation rates may have varied substantially over time, and hiatuses have not been identified but cannot be discounted.

Dinocyst event	**Borehole depth (m)**	**Age (Period)**	**Age (Ma)**	**Location**	**Reference**
Acme *Impagidinium Multiplexum*	150	Early Pleistocene, MIS 97 (Unit N2b)	2.45	Netherlands, North Sea	Meijer et al., 2006
Depleted dinocysts, presence of *Habibacysta Tectata* and absence of Piacenzian dinocysts	153	Early Pleistocene, MIS 98 (Unit N2a)	2.48	Netherlands, North Sea	Meijer et al., 2006
LOD *Barssidinium Pliocenicum*	190	Late Pliocene	2.6	Belgium, North Sea	Louwye et al., 2004
LOD *O.? Eirikianum*	205	Late Pliocene	2.6	Eastern North Atlantic, DSDP 610A	De Schepper et al., 2015
HOD *Invertocysta Lacrymosa*	265	Late Pliocene	2.75 2.8	Eastern North Atlantic, DSDP 610A Singa section, Italy	S.D.S. and M.J.H., unpub. Data Versteegh, 1997
LOD *M. choanophorum*	330	Mid Pliocene	3.6	North Sea	Kuhlmann et al., 2006
LCOD *O. tegilatum*	340	Early Pliocene	3.7 4.5	Eastern North Atlantic, DSDP 610A Iceland Sea, ODP 907A	De Schepper et al., 2015
LOD *Reticulatosphaera actinocoronata*	355	Early Pliocene	4.7 5	Capo Rossello, Italy Central North Atlantic, DSDP 607	Londeix et al., 2007 Mudie, 1987, Versteegh, 1997

Table 1. Dinocyst events with ages (From DC-Flood et al., in prep). Ages correlating to MIS 97 and 98 are based on the Lisieki & Raymo (2005).

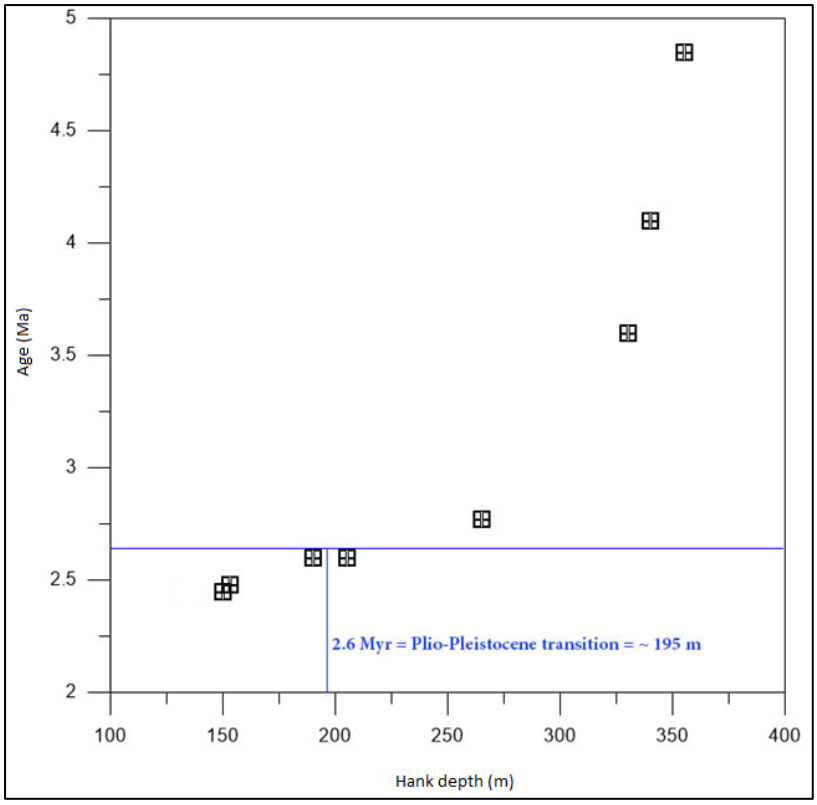

Figure 5. Age points plotted against depth of the Hank core (From: DC-Flood et al., in prep).

2.3. Extraction and lipid analysis

The samples were powdered, homogenized, and extracted with a Dionex Accelerated Solvent Extractor 350 using a 9:1 (v/v) mixture of dichloromethane and methanol. The total lipid extracts were separated into apolar, neutral and polar fractions over an activated Al_2O_3 column using hexane:DCM (9:1, v/v), hexane:DCM (1:1, v/v), and DCM:MeOH (1:1, v/v), respectively. Neutral fractions, containing alkenones, were analyzed using Gas Chromatography Flame Ionization Detection (GC-FID). Polar fractions, containing GDGTs and diols, were first analyzed using high-performance liquid chromatography/atmospheric pressure chemical ionization-mass spectrometry (HPLC-APCI-MS) using an Agilent 1290 HPLC-MSD SL at Utrecht University. Single-ion monitoring (SIM) was used to quantify the abundance of GDGTs. After GDGT analysis, polar fractions were made amenable to gas chromatography by silylation with the addition of N,O-bis(trimethylsilyl)trifluoroacetamide (BSTFA) and pyridine (60 ◦C, 20 min). Long-chain diol distributions were analyzed using a Thermo trace gas chromatograph (GC) Ultra coupled to Thermo DSQ MS at Royal NIOZ. Various long-chain diols were quantified using SIM mode.

2.4. Proxy calculations

Alkenone relative abundances were determined by the integration of relevant peak areas. The $U^{K'}_{37}$ index (Eq. 1) was used to estimate SSTs according to the equation of Prahl and Wakeham (1987):

$$U^{K'}_{37} \text{ index} = [C_{37:2}] / ([C_{37:2}] + [C_{37:3}]) \quad (1)$$

For molecular structures, see Fig. 1. $U^{K'}_{37}$ values were converted to SSTs using the global core top calibration of Müller et al. (1998):

$$U^{K'}_{37} = 0.033 \times SST + 0.044 \quad (2)$$

The calibration error associated with the $U^{K'}_{37}$ is 1.5 °C (Müller et al., 1998).

The identification and quantification of the GDGT isomers was achieved by integrating the peak areas of relevant peaks in m/z 1302, 1300, 1298, 1296, 1292, 1050, 1036, 1022 and 744 mass chromatograms. The TEX_{86}^{H} index was calculated following Kim et al. (2010):

$$TEX_{86}^{H} = \log (([GDGT\text{-}2] + [GDGT\text{-}3] + [Cren']) / ([GDGT\text{-}1] + [GDGT\text{-}2] + [GDGT\text{-}3] + [Cren'])) \quad (3)$$

For molecular structures, see Fig. 2. TEX_{86}^{H} values were converted to SSTs using the global core top calibration of Kim et al. (2010):

$$SST = 68.4 * TEX_{86}^{H} + 38.6 \quad (4)$$

The calibration error associated with the TEX_{86}^{H} is 2.5°C (Kim et al., 2010). The TEX_{86}^{H} index is used as Kim et al. (2010) recommended its use for paleotemperatures exceeding 15°C, which is expected for the Pliocene North Sea.

Long-chain diols were quantified using an SIM of m/z 299, 313, 327 and 341. The Long-chain Diol Index (LDI) was calculated and converted to SST following Rampen et al. (2012):

$$LDI = [C_{30}\ 1,15] / ([C_{28}\ 1,13] + [C_{30}\ 1,13] + [C_{30}\ 1,15]) \quad (5)$$

$$LDI = 0.033 * SST + 0.095 \quad (6)$$

For molecular structures, see Fig. 3. The calibration error for the LDI is 2.0 °C (Rampen et al., 2012).

SST results were removed if relevant peaks were not distinguishable, if measured peaks were below detection limit and, in case of the TEX_{86}^{H}, if the BIT index was above 0.3. The BIT index was calculated according to Hopmans et al. (2004):

$$BIT = ([GDGT\text{-}Ia] + [GDGT\text{-}IIa] + [GDGT\text{-}IIIa]) / ([Cren] + [GDGT\text{-}Ia] + [GDGT\text{-}IIa] + [GDGT\text{-}IIIa]) \quad (7)$$

For molecular structures, see Fig. 2.

The %C32 was calculated according to Lattaud et al. (2016):

$$\%C32 = [C_{32}\ 1,15] / ([C_{32}\ 1,15] + [C_{30}\ 1,15] + [C_{30}\ 1,13] + [C_{28}\ 1,13]) * 100\% \quad (8)$$

For molecular structures, see Fig. 3.

2.5. Cyclicity

Spectral analysis methods were conducted on the $U^{K'}_{37}$ dataset in the depth domain with the software package AnalySeries (Paillard et al., 1996). Blackman Tukey spectral analysis was used to identify dominant periodicities present within the data, which were then filtered using a Gaussian filter using AnalySeries. AnalySeries is also used to create a time series of the $U^{K'}_{37}$ record, based on the LOCs of dinoflagellates, after which Blackman Tukey spectral analysis was used to identify dominant periodicities in the age domain, which were also filtered using a Gaussian filter.

2.6. Alkenone stable carbon isotope analysis

Ten samples were selected for alkenone stable carbon isotope analysis. First, alkenone-containing samples were injected on GC-FID system to determine if they contained sulphur. Sulphur-containing samples were stirred overnight with activated copper, filtered over a small column containing Na_2SO_4, and dried under a stream of N_2.

The stable carbon isotopic composition of the C_{37} di-unsaturated alkenone ($\delta^{13}C_{C37:2}$) was measured in duplicate using a GC-isotope ratio monitoring (IRM) MS system with an Agilent 6890 GC coupled to a Thermo Science Delta V isotope mass spectrometer. Results were discarded if the duplicate measurements differed more than one per mill, and if the $C_{37:2}$ alkenone peak could not be quantified properly (below detection limit or not base line separated from other peaks).

2.7. Bulk elemental analysis

Total organic carbon (TOC) content, stable carbon isotopes of the bulk OC ($\delta^{13}C_{org}$), and bulk carbonate ($\delta^{13}C$) was measured for the ten samples selected for alkenone stable carbon isotope

analysis. For the TOC and bulk OC measurements, homogenized sediments were decalcified by overnight treatment with 1.0 M HCl. The samples were then rinsed 2x with demineralised water, and left to dry in an oven (60 °C). TOC content was analyzed online with a CNS-analyzer (NA 1500) following standard procedures. TOC content values are expressed as the weight percentage of dried sediment (wt. %). $\delta^{13}C_{org}$ values were subsequently measured by Elemental Analyzer Continuous Flow Isotope ratio Mass Spectrometry using a Fisons 1500 NCS Elemental Analyzer coupled to a Finnegan Mat Delta Plus mass spectrometer. $\delta^{13}C_{org}$ values are reported in the standard delta notation relative to the Vienna Pee Dee Belemnite (VPDB) standard. Bulk carbonate $\delta^{13}C$ was measured on an untreated sample with a GasBench-II coupled to a Thermo Delta-V advantage isotope ratio mass spectrometer. A mass balance was used to calculate inorganic carbon $\delta^{13}C$.

2.8. Alkenone pCO_2 estimates

Estimation of atmospheric pCO_2 concentrations from $\delta^{13}C_{C37:2}$ is done via three steps, following the approach of Bijl et al. (2010). First, the fractionation factor during photosynthesis (ε_p) of haptophyte algae is calculated using two values: δ_p and δ_d. δ_p is the carbon isotopic composition of haptophyte organic matter, which is enriched in ^{13}C by 4.2‰ relative to $\delta^{13}C_{C37:2}$. δ_d is the $\delta^{13}C$ value of dissolved CO_2 ($\delta^{13}C_{CO2(aq)}$), which can be derived from the $\delta^{13}C$ of bulk carbonate with the carbon fractionation factors from biogenic calcite to gaseous CO_2. The fractionation factors depend on sea surface temperature, therefore alkenone-derived $U^{K'}_{37}$ SSTs are used to reconstruct $\delta^{13}C_{CO2(aq)}$ (δ_d). Step two involves estimating $[CO_{2(aq)}]$ from ε_p. According to Pagani (2002) and Pagani et al. (2005), ε_p varies as a function of $[CO_{2(aq)}]$, the carbon isotopic fractionation due to carboxylation (ε_f), specific cell physiological parameters and other environmental parameters, primarily light intensity. ε_f is ~25‰ in the modern day ocean, and is assumed to be constant (Popp et al., 1998, Pagani, 2002). The sum of all physiological factors is described by surface water concentration of phosphate ($[PO_4^{3-}]$), as it is a limiting nutrient for productivity, or it serves as a proxy for other limiting nutrients (Bijl et al., 2010, Pagani et al., 2005). Therefore, $[CO_{2(aq)}]$ can be calculated with ε_p, ε_f and $[PO_4^{3-}]$. $[PO_4^{3-}]$ is 0.6 ± 0.2 in the modern day North Sea, according to the World Ocean Atlas 2005 (Baranova, 2015) and assumed to be similar in the Pliocene. Due to the shallow depth of the North Sea, $[CO_{2(aq)}]$ in this setting depends primarily on atmospheric CO_2 concentrations (pCO_2). The third and last step is therefore the conversion of $[CO_{2(aq)}]$ to pCO_2 with Henry's Law (Weiss, 1974), for which the SST and sea surface salinity (SSS) are needed. $U^{K'}_{37}$ based SSTs, and a constant SSS of 34 PSU (modern day North Sea; Baranova, 2015) are used for this (the SSS of the Pliocene North Sea is assumed to be similar to the modern day North Sea).

3. Results

3.1. Age model and lithology

Based on the age model, the studied interval of the Hank core approximately spans the Zanclean and Piacenzian (Pliocene, 5.3 – 2.6 Ma) and part of the Gelasian (Pleistocene) until ~2.5 Ma (Fig. 5). The BIT index (see section 4.4) indicates the approximate location of the Pliocene – Pleistocene transition (2.6 Ma) at ~195 m. Lithology (Fig. 6) possibly represents distance to the coast, therefore likely indicates sea level changes. As sand is the main lithology, sandy shells could indicate more proximal circumstances and clay and loam more distal circumstances. The distinct clay layer at 291 – 271 m falls within the interval between 296 – 258 m with high resolution SST data (see section 3.2). As this

interval contains warm mean air temperatures (see section 4.4), and as it seems to be around ~3 Ma according to the age model, this interval is referred to as the Mid-Pliocene Warm Period (MPWP) in this thesis. The interval between 404 – 330 m, with high sedimentation rates and/or many unknown hiatuses, is referred to as the early Pliocene. The interval between 330 – 195 m, with lower sedimentation rates, is referred to as the late Pliocene. The interval between 195 – 178 m is referred to as the Pleistocene.

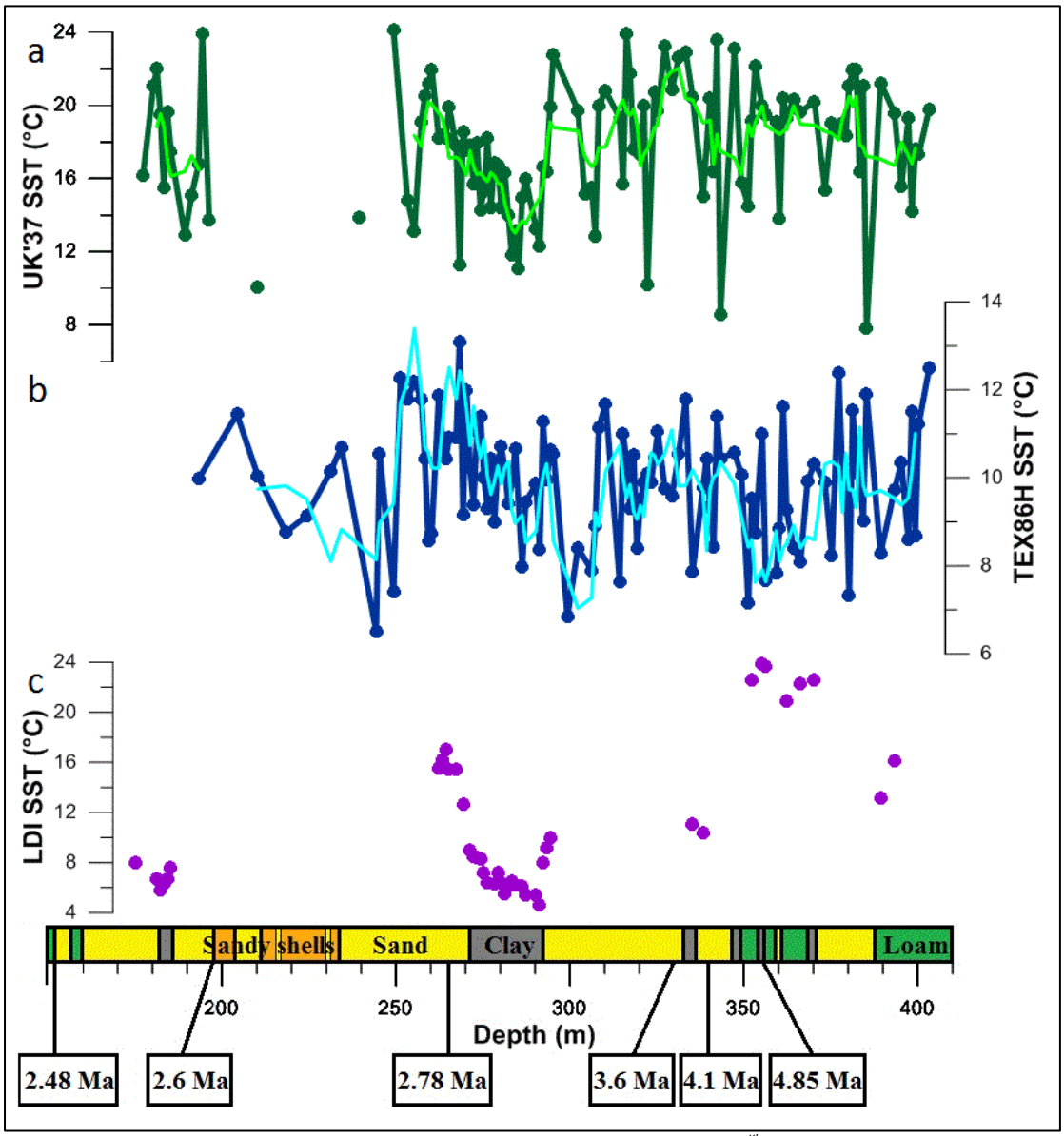

Figure 6. Reconstructed sea surface temperatures for the Pliocene. (a) SSTs based on the $U^{K'}_{37}$ proxy. Light green line represents a five point moving average. (b) SSTs based on the TEX_{86}^{H} proxy. Bright blue line represents a five point moving average. (c) SSTs based on the LDI proxy.

3.2. Sea surface temperature proxy comparison

The three SST records are presented in Fig. 6. All three records show large fluctuations on a scale of 1 – 5 m, now on referred to as short scale. SSTs based on $U^{K'}_{37}$ fluctuate between 8 and 24°C, SSTs based on TEX_{86}^{H} fluctuate between 6 and 13°C and SSTs based on LDI fluctuate between 4 and 24°C. No clear trend is seen over the whole record, apart from large variation on short scale, SSTs over the Pliocene seem to be stable. Short scale fluctuations in the $U^{K'}_{37}$ record and the TEX_{86}^{H} record appear to

occur on the same scale. Between 296 – 258 m (MPWP), all three SST records are relatively high resolution in terms of number of data points, and seem to show the same trend of rising temperatures. To compare the records, regression analysis is applied. This is completed twice: once for the whole record (Fig. 7), and once for the MPWP interval (Fig. 8).

Over the whole record, the SSTs based on LDI and $U^{K'}_{37}$ correlate, with an R^2 of 0.34. The SSTs based on TEX_{86}^{H} do not correlate with the LDI SSTs (R^2 of 0.00), and do not correlate with the $U^{K'}_{37}$ SSTs (R^2 of 0.02) (Fig. 7). The correlation between SST derived with LDI and $U^{K'}_{37}$ over the MPWP strengthens compared to the correlation over the whole record, and shows an R^2 of 0.46. SSTs derived with TEX_{86}^{H} and LDI in the MPWP show a weak correlation with an R^2 of 0.26. SSTs derived with TEX_{86}^{H} and $U^{K'}_{37}$ in the MPWP do not correlate (R^2 of 0.00) (Fig. 8).

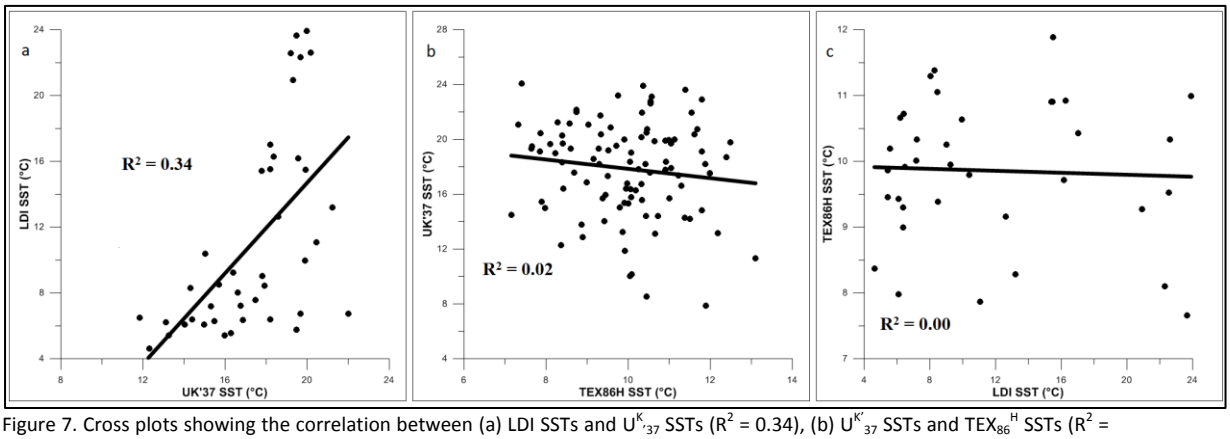

Figure 7. Cross plots showing the correlation between (a) LDI SSTs and $U^{K'}_{37}$ SSTs (R^2 = 0.34), (b) $U^{K'}_{37}$ SSTs and TEX_{86}^{H} SSTs (R^2 = 0.02), and (c) TEX_{86}^{H} SSTs and LDI SSTs (R^2 = 0.00).

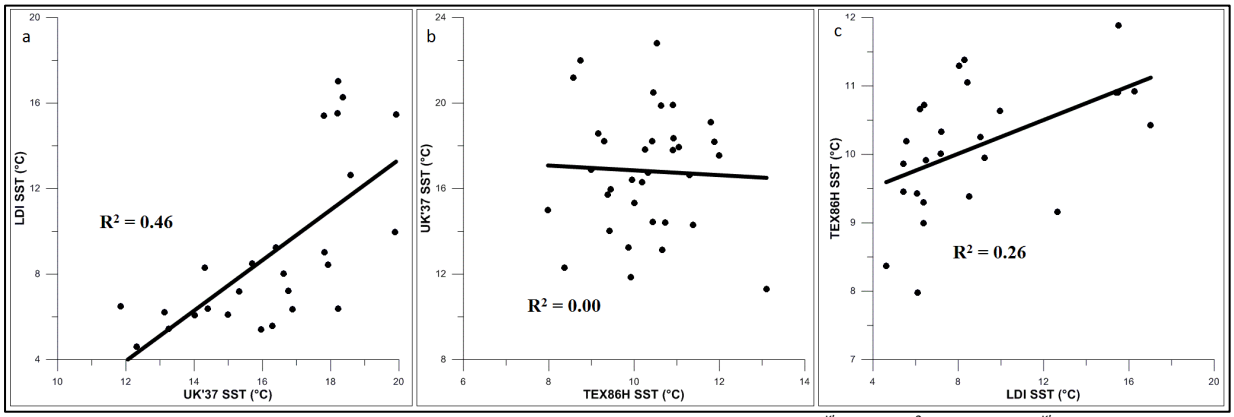

Figure 8. Cross plots showing the correlation in the MPWP interval between (a) LDI SSTs and $U^{K'}_{37}$ SSTs (R^2 = 0.46), (b) $U^{K'}_{37}$ SSTs and TEX_{86}^{H} SSTs (R^2 = 0.00), and (c) TEX_{86}^{H} SSTs and LDI SSTs (R^2 = 0.26).

3.3. Terrestrial input

Two proxies are used to indicate soil and riverine input, i.e. the Branched over Isoprenoid Tetraether Index (BIT index) and the percentage of the C_{32} 1,15-diol over the sum of all 1,13 and 1,15 diols (%C32), respectively. The BIT index fluctuates between 0.05 and 0.85 throughout the record (Fig. 9). Most of the BIT values are <0.3. BIT values are low in the early part of the record, and increase from 210 m onward towards values of 0.85. Peaks with values >0.3 are observed around 380 m, 300 m and 220 m. The %C32 fluctuates between 20% and 60% (Fig. 9). Variation is seen on short scale (1- 5 m) and three peaks with low values are seen around 380 m, 325 m and 300 m, coinciding with higher BIT index values. %C32 values are lower in the Pleistocene than in the Pliocene and values decrease during the MPWP.

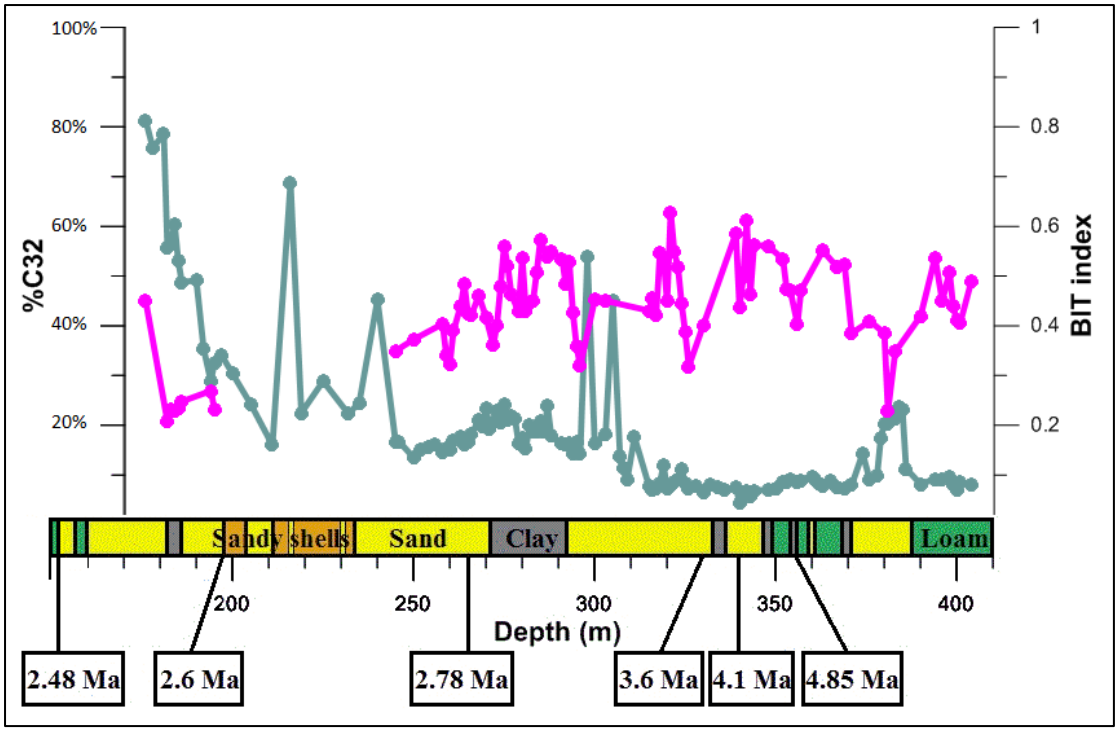

Figure 9. BIT index (green line) and %C32 (pink line).

4. Discussion

4.1.1. SST proxy comparison: differences in absolute values

The absolute values in degrees Celsius of the SSTs derived with the three organic proxies differ substantially (Fig 6). The $U^{K'}_{37}$ derived SSTs show a large variation (16°C) in temperatures. The LDI derived SSTs vary over an even larger range (20°C). The TEX_{86}^{H} derived SSTs show substantially less variation in temperatures (7°C). TEX_{86}^{H} SSTs also possess lower absolute temperatures than the $U^{K'}_{37}$ and LDI derived SSTs (~8 °C lower). A number of reasons for differences in proxy results are presented by several other proxy comparison studies (Lee et al., 2008, Rommerskirchen et al., 2011, Rodrigo-Gámiz et al., 2014, 2015, Plancq et al., 2015). Lower TEX_{86}^{H} than $U^{K'}_{37}$ derived SSTs have been observed in other places. In general, these lower TEX_{86}^{H} SSTs are explained by the observation that TEX_{86}^{H} may in fact be representing subsurface temperatures (Lee et al., 2008, Rommerskirchen et al., 2011, Rodrigo-Gámiz et al., 2015). However, as the Pliocene North Sea is shallow (~100m), the TEX_{86}^{H} proxy cannot reflect a strong subsurface temperature bias. Similarly, the proxies cannot be influenced by upwelling.

Alternatively, the differences in the proxy results for this study may be explained by different production seasons for the biomarker producing organisms. Alkenones are mainly produced in spring (Chapman et al., 1996, Hardee & Thunell, 2007, Rodrigo-Gámiz et al., 2014), whereas GDGTs have a longer production season but are mainly produced in winter (Herfort et al., 2006, Pitcher et al., 2011). This could cause lower TEX_{86}^{H} derived SSTs, which are more smoothed out compared to the $U^{K'}_{37}$ derived SSTs. The source and the seasons of production of long chain diols is not well known to date. Villanueva et al. (2014) found that diol producing algae bloom in multiple seasons. This could perhaps cause the extreme variation in the LDI based temperatures, where the high values in the record could be summer biased and the low values could be winter biased. Nevertheless, even when taking

seasonal biases into account, the three different proxies display large differences. Rodrigo-Gámiz et al. (2014) also explained the offset between LDI and $U^{K'}_{37}$ derived SSTs in the Mediterranean by a seasonal bias, although the offset was substantially smaller (6°C) than in the North Sea (18°C). Due to the relatively shallow water column and latitudinal position, the North Sea experiences large seasonal temperature differences (modern day North Sea summer and winter temperatures are 17 and 6 °C), so that different production seasons of the proxy-biomarkers could result in large variations in reconstructed SSTs.

4.1.2. SST proxy comparison: differences in trends

Whereas differences in absolute proxy values can be explained by seasonal biases, trends on the other hand, are expected to be the same, as the proxies are all expected to capture the same SST signal. To check if the proxies behave similarly, regression analysis is applied (Fig. 7). The LDI and $U^{K'}_{37}$ derived SSTs correlate (r^2 = 0.34), indicating that those two proxies indeed reflect the same general variations in temperatures. However, the TEX_{86}^{H} derived SSTs do not correlate with the SSTs from the $U^{K'}_{37}$ and LDI proxies. Interestingly, the TEX_{86}^{H} record for IODP Site U1313 (North Atlantic) matches that of the $U^{K'}_{37}$ record from the same site (Naafs, personal communication), suggesting that the TEX_{86}^{H} proxy may not be reliable at the Hank site. It is probable that certain local parameters cause the TEX_{86}^{H} proxy to produce a record that does not match the other SST proxies. One possibility may be that the water column is too shallow for TEX_{86}^{H}, but the exact cause of the mismatch remains uncertain.

Regression analysis is also applied on the MPWP interval (258 – 296 m), where the temporal resolution is relatively high compared to the rest of the core (Fig. 8). As expected, in this part of the core, the LDI and $U^{K'}_{37}$ derived SSTs also correlate (r^2 = 0.46), which confirms the reliability of the SST records based on these two proxies. The continued mismatch between TEX_{86}^{H} and $U^{K'}_{37}$ derived SSTs (r^2 = 0.00) confirms that the TEX_{86}^{H} proxy is most likely not reliable in this setting. This is confirmed by the very weak correlation (r^2 = 0.26) between TEX_{86}^{H} and LDI derived SSTs in this interval.

4.2. Large fluctuations in SSTs: comparison with two North Atlantic SST records

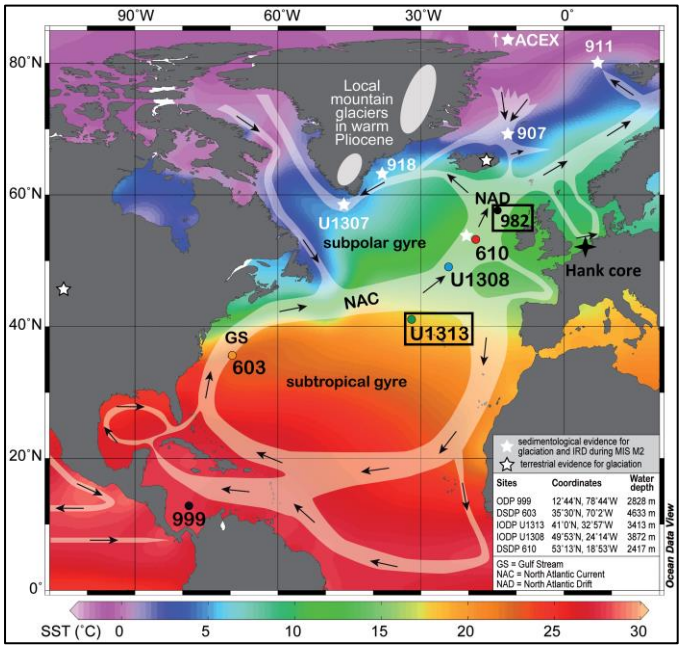

Figure 10. North Atlantic ocean currents, with Site U1313 and Site 982 indicated in the figure. From: De Schepper et al., 2013.

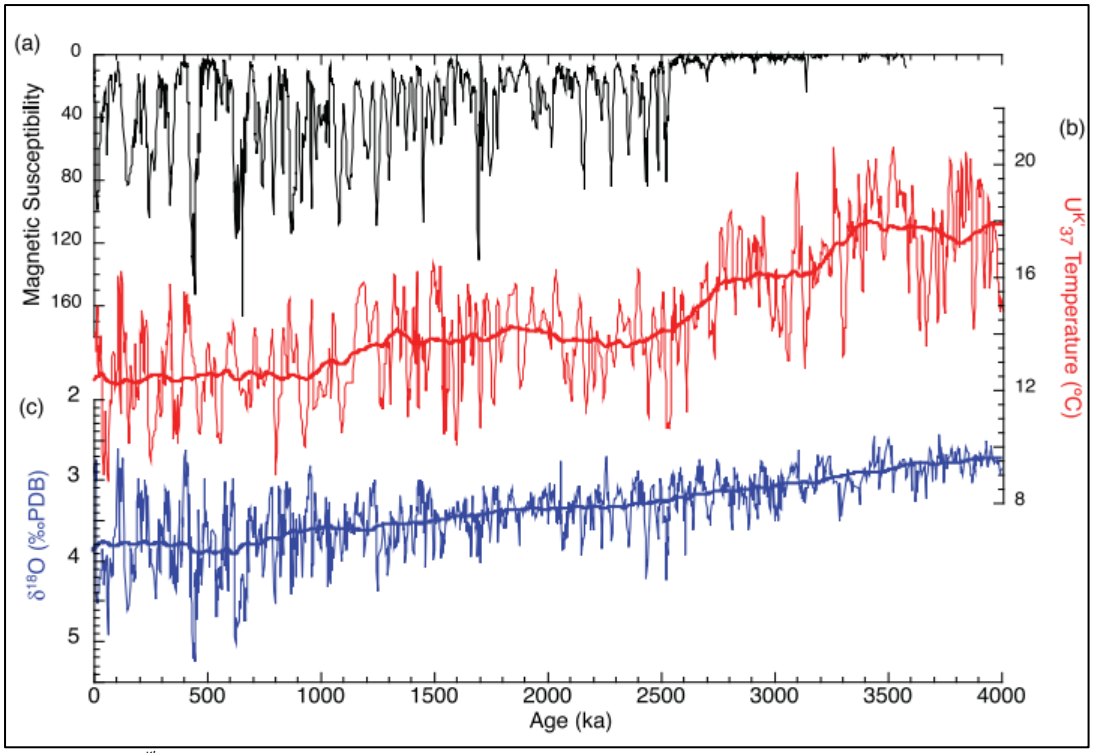

Figure 11. (b) $U^{K'}_{37}$ derived SSTs (°C) from ODP Site 982. The thick red line is a smoothed running means using a 400 kyr (kiloyear) window. From: Lawrence et al. (2009).

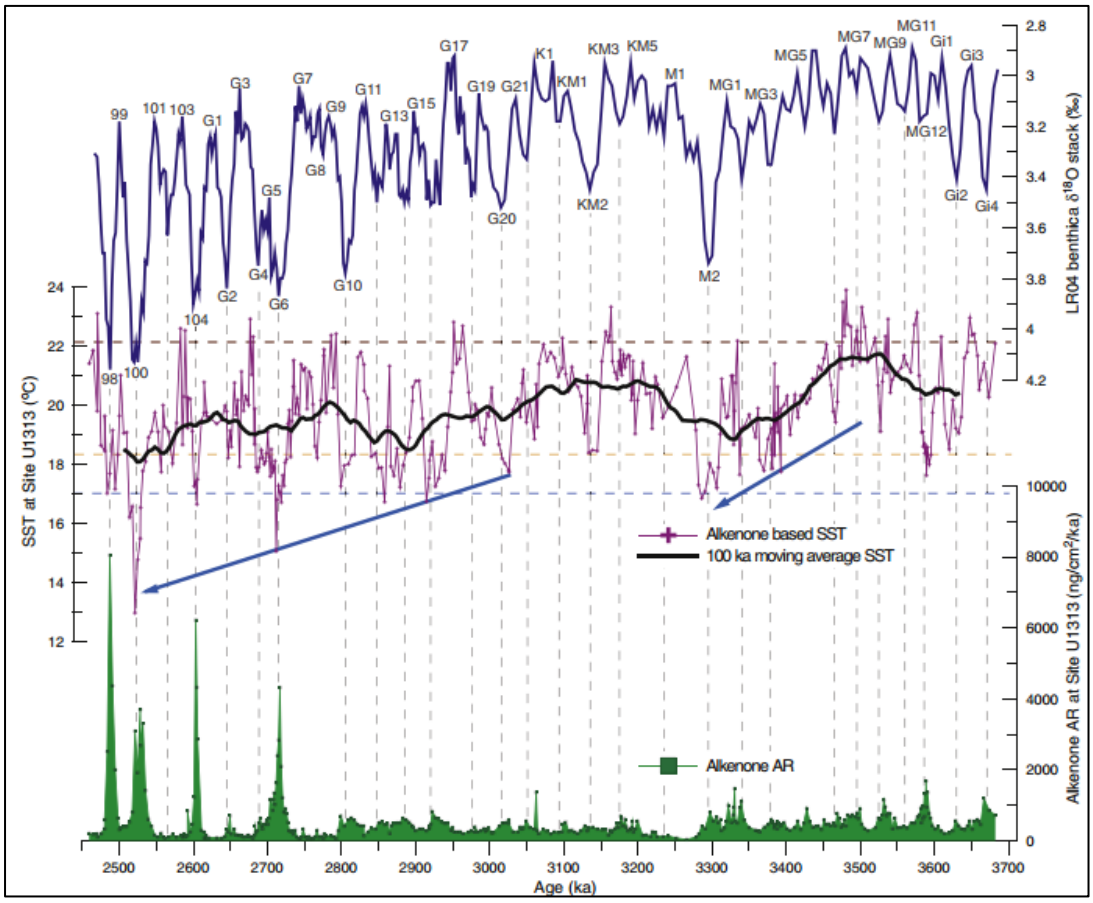

Figure 12. $U^{K'}_{37}$ derived SSTs (purple) from Site U1313. The thick black line is a 100 kyr moving average of the SST record. From: Naafs et al., 2010.

The North Sea SST records show large fluctuations in temperatures on short scale. Two North-Atlantic records (Fig. 10) show similarly large fluctuations in $U^{K'}_{37}$ derived SSTs (Lawrence et al., 2009, Fig. 11, and Naafs et al., 2010, Fig. 12). Lawrence et al. (2009) present reconstructed SSTs for the last 4 Ma from ODP Site 982 (North Atlantic, high latitude). Naafs et al. (2010) present reconstructed SSTs from 3.7-2.5 Ma, from IODP Site U1313 (North Atlantic, mid latitude). Comparing the two records from the North Atlantic with the North Sea record of this study, it can be seen that temperature fluctuations in the three records are in the same order of magnitude, and also that the long term trends between the records are comparable.

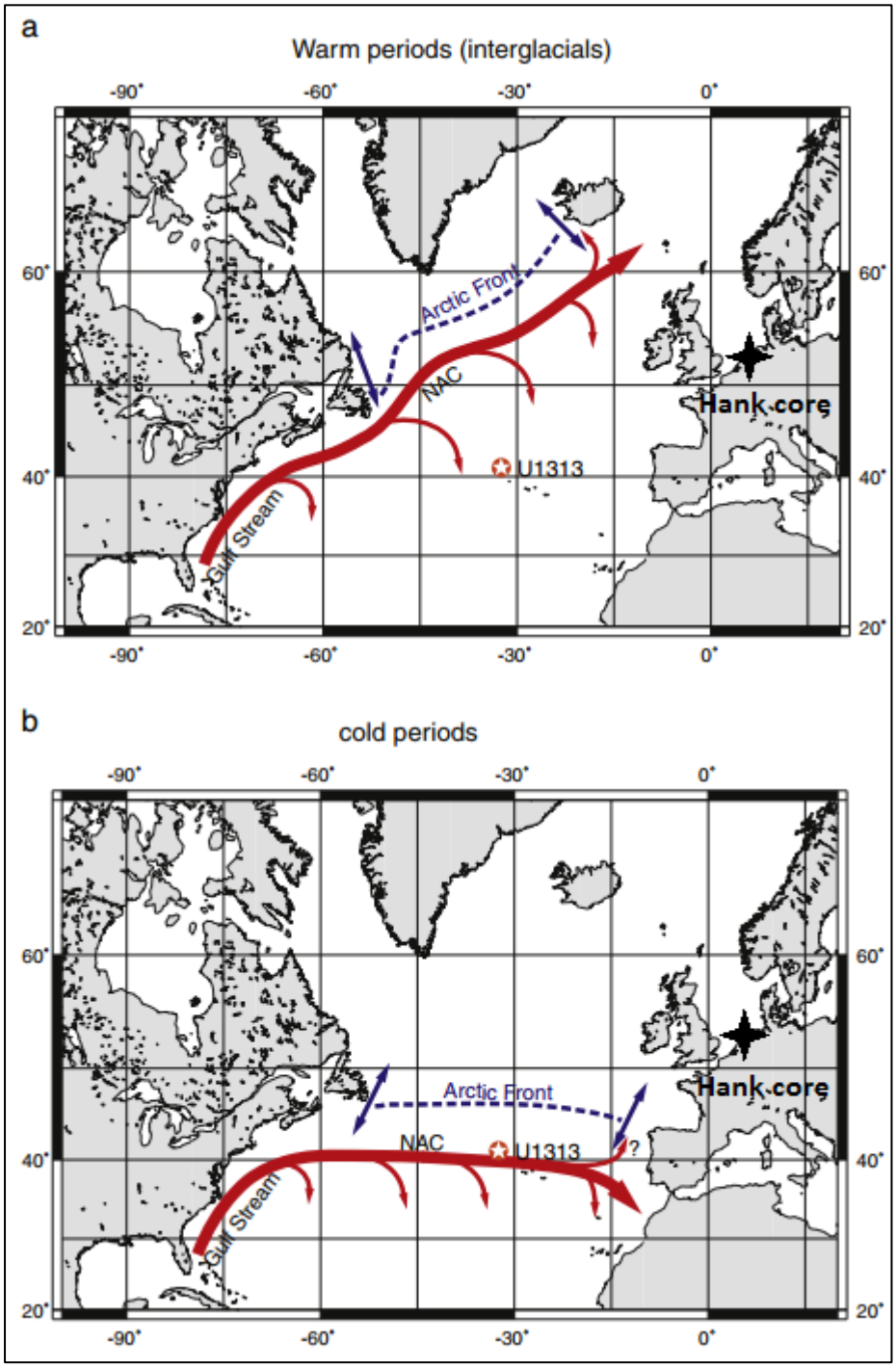

Figure 13. The configuration of the North Atlantic Current and the Arctic Front in warm periods (a) and cold periods (b). From: Naafs et al., 2010.

The running mean of all records, including the records from Site U1313 and ODP Site 982, reflect relatively stable conditions during the Pliocene, preceding a decrease in temperatures prior to the Pleistocene. Lawrence et al. (2009) proposed two scenarios to explain the large fluctuations in SSTs in the Pliocene. The first scenario is that strong regional high-latitude feedbacks to obliquity-induced insolation changes cause the large fluctuation. In the second scenario, changes in the strength and position of the North Atlantic Current (NAC, Fig. 13) caused the large fluctuations. The latter scenario is also proposed by Naafs et al. (2010) as a mechanism for the large fluctuations in the record at Site U1313. The first scenario would only or predominantly influence high-latitudes, and would also cause large fluctuations in temperatures in both the marine and terrestrial environment. The second scenario could affect both high and mid latitudes, and would predominantly influence temperatures in the marine environment. As Naafs et al. (2010) observed large fluctuations in SSTs in the mid latitude Atlantic ocean, the second option seems the most plausible as cause for the large fluctuations in SSTs in the mid and high latitude North Atlantic, and consequently, the North Sea.

Figure 13a shows the current configuration of the North Atlantic Current (NAC; Naafs et al., 2010). The NAC brings warm waters from the Caribbean towards Europe and leads to the relatively mild climate of Western Europe. It is proposed that in cold periods, the NAC shifts eastwards, and the Arctic Front (AF) shifts southwards (Figure 13b). As the North Sea is influenced by the currents of the Atlantic ocean (Fig. 10), the North Sea is influenced by the AF during cold periods, and by the NAC during warm periods. These shifts in ocean surface currents could consequently cause large fluctuations in SSTs in the North Atlantic and the North Sea, whereas deep sea temperatures and terrestrial temperatures would demonstrate lower amplitudes and consequently, less variation. The record of Lawrence et al. (2009) shows slightly larger fluctuations (~6 °C) than the record of Naafs et al. (2010) (~4 °C), which is likely due to increased seasonality on higher latitudes, which also increases the scale of temperature variability. The shallow water mass of the North Sea may have been highly reactive to temperature changes, causing even larger SST differences than the North Atlantic.

Naafs et al., (2010) propose that shifts in the configuration of the NAC could be driven by orbitally induced changes in solar insolation. Fluctuations in insolation at high latitudes, possibly amplified by changes in sea-ice extent, may lead to changes in atmospheric pressure systems and thus alter the strength and position of the westerly winds, which subsequently influences the strength and position of the NAC (Lawrence et al., 2009). According to De Schepper et al. (2013), changes in benthic $\delta^{18}O$, which represent changes in deep sea temperature and global ice volume (Lisiecki & Raymo, 2005), lag with respect to changes in the NAC. This could be because both $\delta^{18}O$ fluctuations and changes in the NAC are driven by orbital variations (Lisiecki & Raymo, 2005), but the configuration of the NAC responds rapidly via wind system shifts, whilst $\delta^{18}O$ fluctuations respond slowly via the growth of continental ice sheets.

In a time with continental ice sheets in the Arctic region, strong feedbacks could cause extreme cold circumstances at high latitudes in glacials, which could force the AF towards the mid latitudes and the NAC to flow eastward. Therefore, the penetration of the Arctic Front towards the mid latitudinal North Atlantic seems likely after the onset of Northern Hemisphere Glaciations (NHG; 2.7 Ma), but it is less plausible that the AF penetrates that far southwards in a time when there were no large continental ice sheets in the Arctic. However, the fact that changes in the NAC lead changes in $\delta^{18}O$, indicates that changes in NAC are initially caused by wind systems and not by continental ice sheet grow and decay. Therefore, no continental ice sheets are needed for shifts in NAC configuration, and those shifts may have also occurred before the onset of NHG. During the late Pliocene, the Arctic was already partially covered by sea ice, which can induce enough feedbacks to cause the AF to penetrate southwards during glacials. The shifts in the configuration of the NAC and the AF were probably less extreme in the late Pliocene compared to the early Pleistocene, with the AF not reaching the mid

latitudinal North Atlantic. But the AF could have influenced the high latitudinal North Atlantic and the North Sea in the late Pliocene. Before the opening of the Bering Strait at 4.5 Ma, it is less likely that cold surface currents influenced the North Sea, as the entire North Atlantic region was influenced by warm currents from the south before 4.5 Ma (De Schepper et al., 2015). It is therefore unclear what has caused the fluctuations in North Sea SSTs before 4.5 Ma.

Lawrence et al. (2009) found variations in SSTs on obliquity scale throughout the Pliocene and early Pleistocene at Site 982 (high latitudinal North Atlantic, Fig. 10). As obliquity is assumed to be the driving force behind temperature fluctuations between 2.7 – 0.8 Ma (Lisiecki & Raymo, 2005), it is probable that obliquity has driven shifts in the NAC throughout this period. It is however remarkable that the SSTs at Site 982 also vary on obliquity scale before 2.7 Ma, because the benthic $\delta^{18}O$ record of Lisiecki & Raymo (2005) varies with eccentricity/precession throughout the Pliocene until 2.7 Ma. Perhaps changes in the configuration of the NAC do not vary on the same scale as deep sea temperatures and global ice volume during the Pliocene. If orbitally driven changes in the NAC influence both the high latitudinal North Atlantic and the North Sea during the Pliocene, the SSTs in the North Sea should vary on the same scale as the SSTs at Site 982 (obliquity).

4.3. Cyclicity in SST fluctuations

The Earth's obliquity fluctuates on a cycle of 41 kyr (kiloyear) (Laskar, 1990). In order to test the hypothesis that North Sea SSTs during the Pliocene and early Pleistocene were driven by obliquity, it is necessary to determine if the fluctuations in the record are on the correct scale (41 kyr). To determine this, spectral analysis is used. However, this record has two restrictions. First, the age model is based on only six data points, and indicates that the sedimentation rate changes substantially over time (Fig. 5). Second, the resolution of the records is not high enough throughout the whole core to recognize the obliquity cycle. To be able to resolve a cycle with spectral analysis, a minimum of two samples per cycle is required. The maximum frequency that can be resolved in a certain domain with a specific amount of data points is called the Nyquist Frequency (Grenander, 1959, Stiltz, 1961).
As Hank's age model is not well constrained, spectral analysis is first applied in the depth domain. All analyses are performed on the $U^{K'}_{37}$ record, which is the most complete, and considered to be the most reliable of the three SST proxy records (see section 4.1.2). Figure 14 shows the power spectrum of the $U^{K'}_{37}$ record. Peaks in the record occur at 7.5 m, 13 m and 17 m (Fig. 14).

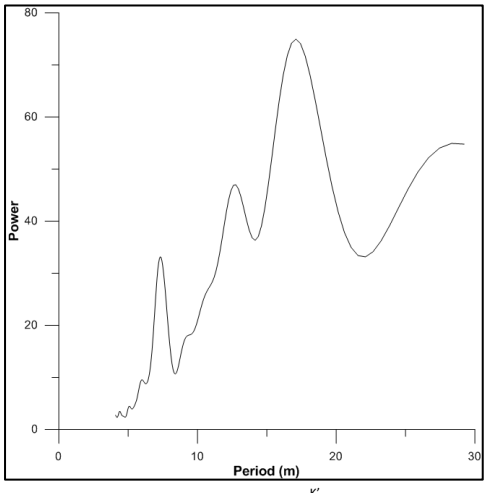

Figure 14. Power spectrum of the $U^{K'}_{37}$ SST record, showing peaks at 7.5 m, 13 m and 17 m.

Because the age model indicates that (a) large fluctuations in sedimentation rate occur over the record, and (b) there may be one or more hiatuses in the record, the 7.5 m signal may not be constant over the record, rendering its interpretation ambiguous. Filtering the $U^{K'}_{37}$ record for the 7.5 m cycle shows that it coincides with the record between 350 – 300 m (Fig. 15). The 7.5 m filter is the strongest (largest amplitude) in that interval, meaning that the 7.5 m cycle has a strong influence there. In other parts of the record, the amplitude of the filter is weak, meaning that the cycle is hardly observable in those intervals.

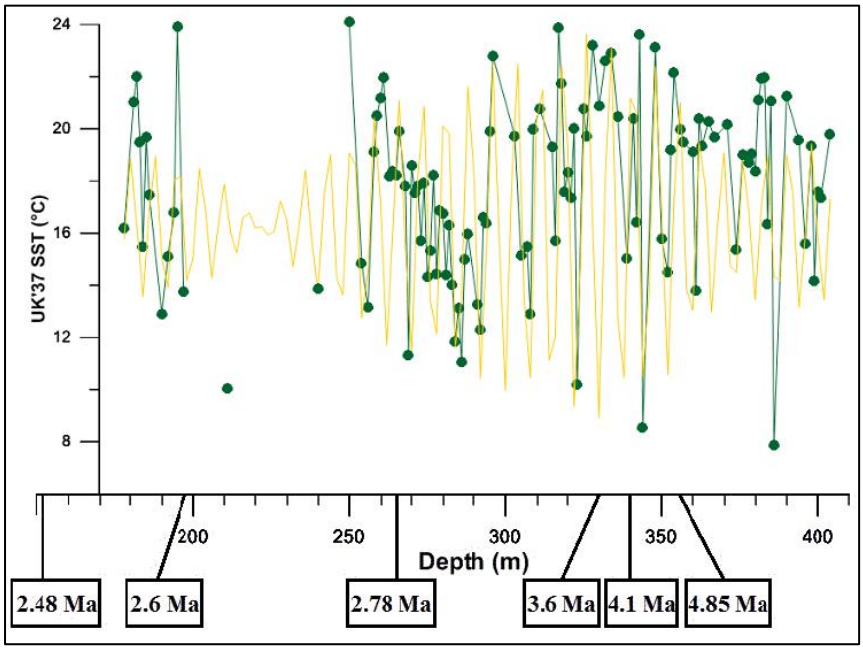

Figure 15. The $U^{K'}_{37}$ SST record (green line) and a 7.5 m Gaussian filter of the $U^{K'}_{37}$ SST record (yellow line).

A time series is made based on the six age points of the $U^{K'}_{37}$ record. Due to the low sedimentation rate in the oldest part of the Pliocene (until 330 m or 3.6 Ma), that part of the record is unreliable and the Nyquist Frequency is too high to solve Milankovitch scale cyclicity. Therefore, the younger part of the record is chosen for analysis. Two intervals were chosen: the MPWP, 296-258 m (or 3.17 - 2.76 Ma), and the late Pliocene, 330-178 m (or 3.6 – 2.55 Ma). The resolution of both intervals is high enough to solve the obliquity cycle of 41 kyr according to the Nyquist frequency of the intervals. The Nyquist frequencies of the MPWP and the late Pliocene correspond to a cycle of ~30 kyr.

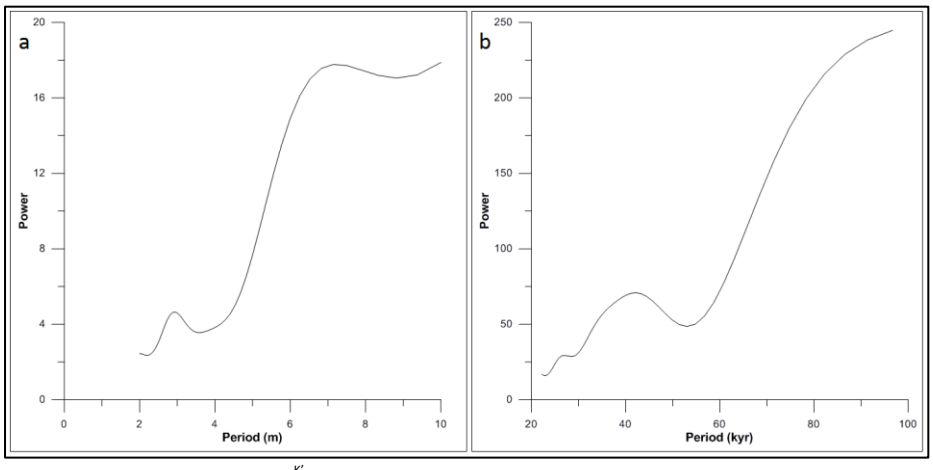

Figure 16. Power spectra of the $U^{K'}_{37}$ SST record of the MPWP interval in the depth domain, showing a clear cycle of ~3 m and a weak cycle of ~7m (a), and in the age domain, showing a clear cycle of 42 kyr (b).

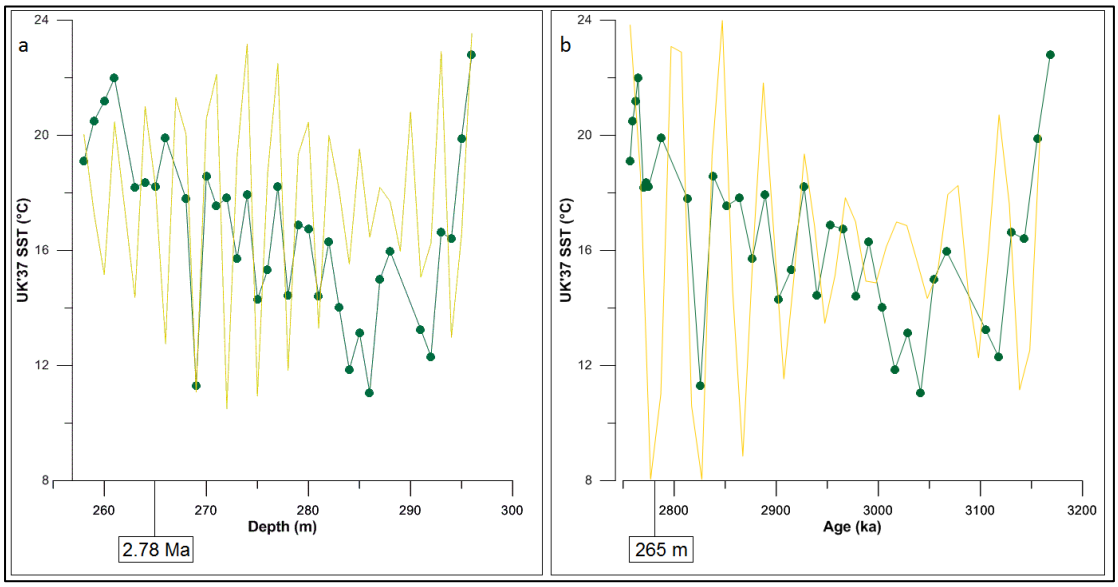

Figure 17. (a) The $U^{K'}_{37}$ SST record of the MPWP interval in the depth domain (green line) and a 3 m Gaussian filter of the UK'37 SST record (yellow line). (b) The $U^{K'}_{37}$ SST record of the MPWP interval in the age domain (green line) and a 43 kyr Gaussian filter of the $U^{K'}_{37}$ SST record (yellow line).

The MPWP shows a cyclicity of 3 m (Fig. 16a), corresponding to 43 kyr (Fig. 16b). As the MPWP gives a cycle of ~43 kyr and the filtered record matches the $U^{K'}_{37}$ record, I can conclude that temperature changes are obliquity driven in this part of the record. The filtered record matches the $U^{K'}_{37}$ SST record the best in the interval between 2.9 and 2.75 Ma (Fig. 17b). However, the sedimentation rate is likely not constant, leading to the mismatch of the filtered record with the $U^{K'}_{37}$ record between 3.05 and 2.95 Ma. There are ~8 obliquity cycles seen in the MPWP interval (Fig. 17b), which, when assuming one cycle is 41 kyr, gives a total duration of 328 kyr for the interval. This matches the known duration of the MPWP (~300 kyr; Dowsett et al., 2010).

The second power spectrum analysis is performed on the late Pliocene. This interval is only analysed in the age domain. As data points of this interval are less evenly spread in the depth domain than in the age domain (because of changing sedimentation rates throughout this interval), it is possible to solve shorter cycles in the age domain than in the depth domain, according to the Nyquist frequency.

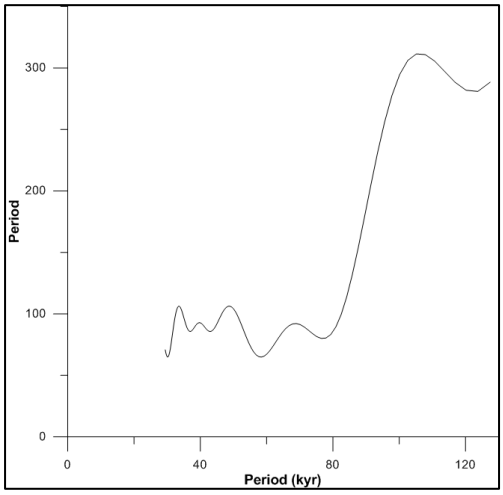

Figure 18. Power spectrum of the $U^{K'}_{37}$ SST record of the late Pliocene interval in the age domain, showing peaks at 34 kyr, 42 kyr, 49 kyr and 108 kyr.

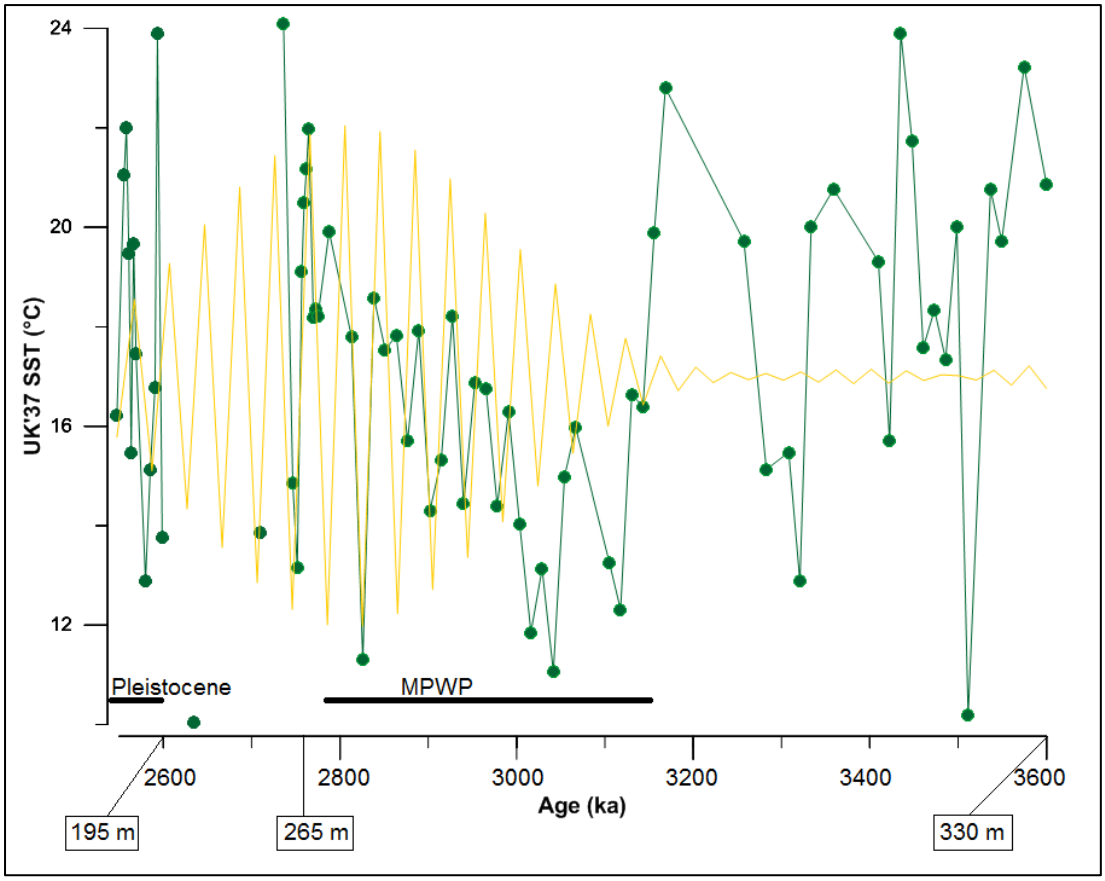

Figure 19. The $U^{K'}_{37}$ SST record of the late Pliocene interval in the age domain (green line) and a 42 kyr Gaussian filter of the UK'37 SST record (yellow line).

The power spectrum possesses peaks at 34 kyr, 42 kyr, 49 kyr and 108 kyr (Fig. 18). First, the $U^{K'}_{37}$ record is filtered for the 42 kyr obliquity cycle (Fig. 19). This filter is very strong in the MPWP, as expected, and in the Pleistocene. The filter is also visible in the gap without data between the MPWP and the Pleistocene, because the gap is small enough for the strong filter to overcome. However, the filter is completely absent in the older part of the interval. From this filtered record, I can conclude that temperature changes from 3.1 Ma toward the Pleistocene are obliquity driven, as the obliquity cycle is strong in this interval. I can also conclude that the obliquity cycle is not found in the older part of the record. Two explanations could account for this: temperature changes may not be obliquity driven in that interval, or the record is not constant and complete enough to show this cycle. Regarding interpretation of the other peaks in the spectrum, the peak at 108 kyr can perhaps represent the eccentricity cycle of Milankovitch. The peaks at 49 kyr and 34 kyr can be harmonics of the eccentricity cycle (½ cycle and ⅓ cycle). The record is filtered for 108 kyr and for 49 kyr and 34 kyr. The cycle of 34 kyr is very close to the Nyquist Frequency (which corresponds to 30 kyr), so this cycle must be analysed with caution. The 108 kyr cycle is present throughout the younger Pliocene, but is strongest in the oldest part (Fig. 20a). This possibly implies temperature changes driven by eccentricity, occur the strongest in the interval where the obliquity cycle is absent. The 49 kyr filter shows the same pattern as the 108 kyr filter, so represents half the eccentricity cycle (Fig. 20b). The 34 kyr filter probably represents ⅓ of the 108 kyr cycle, however this is not very clear, probably because the 34 kyr cycle is too close to the Nyquist Frequency.

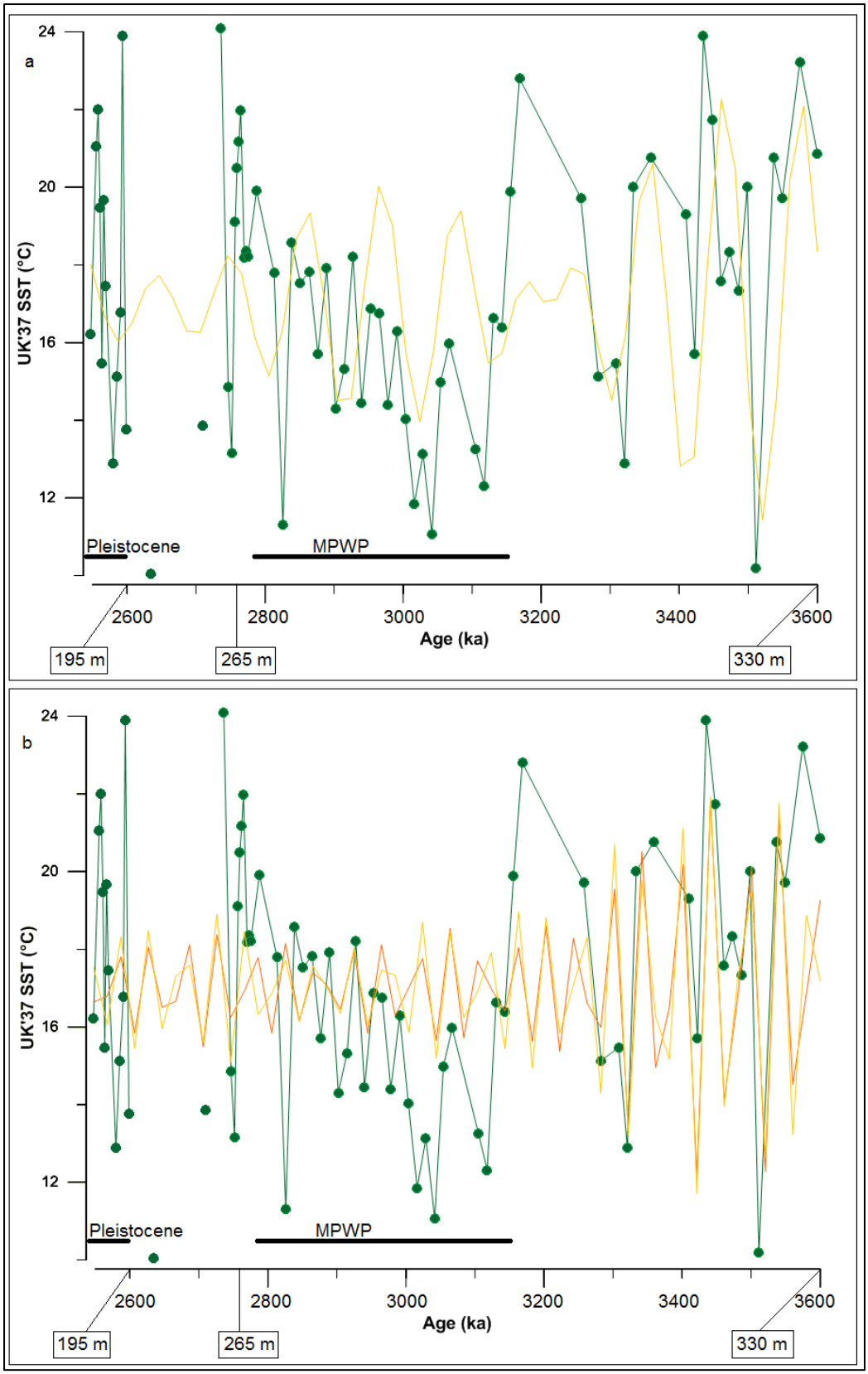

Figure 20. (a) The $U^{K'}_{37}$ SST record of the late Pliocene interval in the age domain (green line) and a 108 kyr Gaussian filter of the UK'37 SST record (yellow line). (b) The $U^{K'}_{37}$ SST record of the late Pliocene interval in the age domain (green line), a 49 kyr Gaussian filter of the $U^{K'}_{37}$ SST record (orange line) and a 34 kyr Gaussian filter of the UK'37 SST record (yellow line).

During the MPWP we can state with certainty that SST temperature changes are driven by obliquity. In the older part of the record, cyclicity becomes less apparent. The obliquity cycle may be absent

because obliquity is not influencing temperature changes there, or the record may not be complete enough to show this cycle. Eccentricity also has a possible effect on temperature. A clear shift is visible at 3.1 Ma: before that age, eccentricity appears to be dominant, and afterwards, obliquity is dominant. This is interesting, because Lisiecki & Raymo (2005) show a shift towards obliquity dominance occurring at 2.7 Ma in Pliocene/Pleistocene benthic $\delta^{18}O$ records. If the shift at 3.1 Ma in my record is a true artefact, and not caused by the incompleteness of the record and changes in sedimentation rate, it raises an interesting question as to why the obliquity becomes dominant from 3.1 Ma. It is certainly not due to the fact that the 100 kyr eccentricity cycle exerts a weak effect there (Fig. 21; Laskar, 1990). In fact, the 100 kyr eccentricity cycle is strong during the MPWP, and the obliquity cycle is weak. Only at around 2.7 Ma does the 100 kyr eccentricity cycle become weak, which can cause the obliquity cycle to become dominant in driving global temperature changes. Therefore, I propose that obliquity and eccentricity both influence temperature changes throughout the whole North Sea SST record, but obliquity is not observable in the older part of the record due to low sample resolution.

As both high latitudinal North Atlantic SSTs (Lawrence et al., 2009) and North Sea SSTs (this study) seem to vary at obliquity scale during the late Pliocene, whilst deep sea temperatures (Lisiecki & Raymo, 2005) vary at precession/eccentricity scale during the late Pliocene until 2.7 Ma, the obliquity driven variations in SSTs are probably a regional phenomenon. It seems likely that the changes in the configurations of the NAC are driven by other orbital forces operating differently to those causing variations in the deep sea temperatures of the late Pliocene.

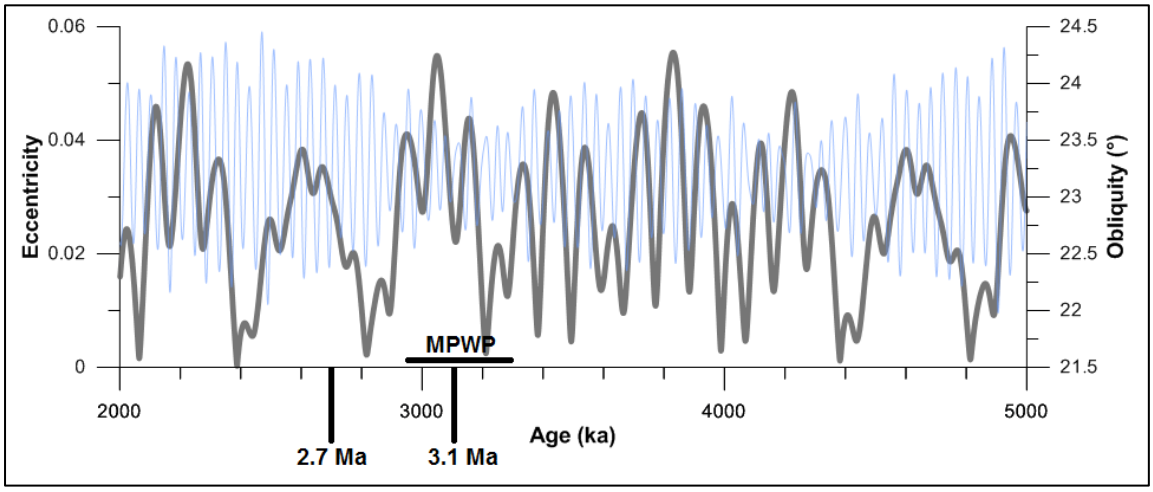

Figure 21. Obliquity (blue) and eccentricity (grey) from 5 – 2 Ma (Laskar, 1990).

4.4. Comparison of the SST records with terrestrial climate and depositional environment

To improve understanding of the reliability of the SST records, I tried to find out more about the depositional environment via the BIT index and the %C32. The Branched over Isoprenoid Tetraether (BIT) index is based on the ratio of terrestrial soil (branched) GDGTs over the total of marine (isoprenoid) and terrestrial GDGTs and is therefore used as a proxy for terrestrial input in a marine environment (Hopmans et al., 2004). The %C32 is based on the ratio of the riverine C_{32} 1,15-diol over the total amount of marine and riverine diols (Lattaud et al., 2016) and could therefore indicate the same as the BIT index. The %C32 is a new proxy and is not yet applied in paleoenvironments. Furthermore, the SST records are compared with the Mean annual Air Temperature (MAT) record of

the same site, which is reconstructed with branched GDGTs by DC-Flood et al. (in prep), to compare the marine climate with the terrestrial climate.

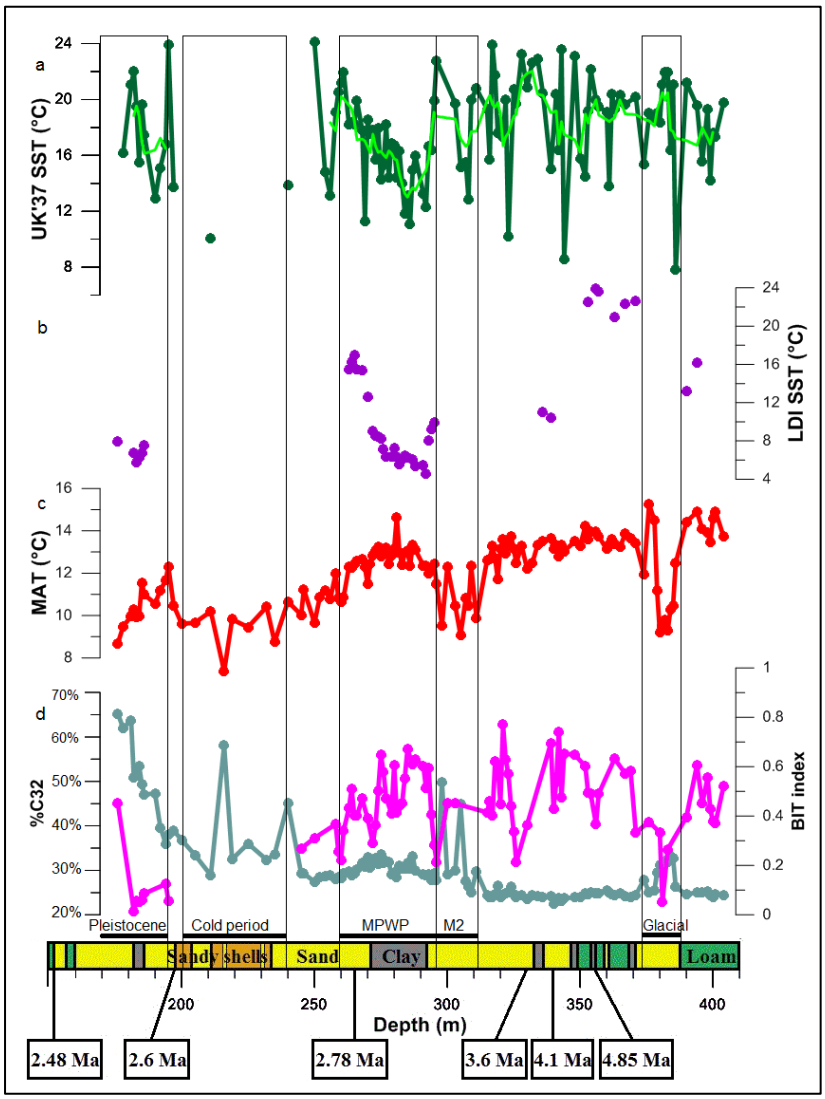

Figure 22. (a) SSTs based on the $U^{K'}_{37}$ proxy. Light green line represents a five point moving average. (b) SSTs based on the LDI proxy. (c) Mean air temperatures based on branched GDGTs (DC-Flood et al., in prep). (d) BIT index and %C32.

Figure 22 shows the $U^{K'}_{37}$ (a) and LDI (b) SST records, the MAT record of the Pliocene (DC-Flood et al., in prep) (c), the BIT index (d) and the %C32 (e). The terrestrial climate record of North Western Europe seems to match the climate evolution that is expected during the Pliocene (Dowsett et al., 2012, Lisiecki & Raymo, 2005). The MAT record (Fig. 22c) shows a relatively stable climate over the Pliocene, and a temperatures decrease towards the Pleistocene. Fluctuations on short scale (1 – 5 m) are seen and seem to occur on the same scale as the fluctuations in the SST records. However, the amplitude of variation in the MAT record (ΔT = 3 °C) is several times smaller than the amplitude of variation in the SST records.

The BIT index (Fig. 22d) for the Pliocene shows values between 0.05 and 0.3, with a few higher values between 0.3 and 0.85. The BIT index increases to values of 0.85 towards the Pleistocene. The %C32 (Fig. 22d) fluctuates between 20% and 60%, is relatively stable during the Pliocene and decreases towards the Pleistocene. The records of the BIT index and the %C32 are expected to correlate in a positive manner, as they should both indicate input from land. Indeed, Lattaud et al. (2016) found a

positive correlation between the %C32 and the BIT index in modern shelf seas. Remarkably, the two terrestrial input indicators do not show the same correlation in this study. Indeed, the cross plot shows a negative correlation between the %C32 and the BIT index (R^2 = 0.27; Fig. 23). To investigate this negative correlation further, absolute values of marine and terrestrial biomarkers (GDGTs and diols) are plotted (Fig. 24), and regression analysis was applied (Fig. 25). The amount of all branched (terrestrial) GDGTs over the record is relatively stable compared to the amount of the marine GDGT crenarchaeol (Fig. 24a). This implies that the BIT index mainly represents fluctuations in marine GDGTs, because these fluctuate with a larger order of magnitude than the terrestrial GDGTs. The amount of the riverine diol C_{32} 1,15 and the amount of all marine diols fluctuate with the same order of magnitude (Fig. 24b). This implies that the %C32 represents fluctuations in both marine and terrestrial diols. The absolute concentrations of marine end-members of these two proxies, the total of marine diols and crenarchaeol, do not correlate (R^2 = 0.00; Fig. 25a). Fluctuations in the absolute amounts of these marine end-members have therefore no common driver. However, absolute concentrations of terrestrial end-members of these two proxies, the C_{32} 1,15-diol and the total of branched GDGTs, do correlate (R^2 = 0.44; Fig. 25b), confirming that these terrestrial end-members do have a common driver: terrestrial input. These findings lead to the following conclusions. The BIT index mainly represents fluctuations in the amount of crenarchaeol. More marine GDGTs are believed to be produced in more marine circumstances and therefore the BIT index is in this case an indicator of sea level fluctuations. The %C32 represents the relative amount of riverine diols over all diols and is therefore an indicator of riverine input in the marine environment. In this case, the negative correlation between the two proxies is probably caused by cold and dry (glacial) circumstances, with little river input (low %C32) and low sea level (high BIT index). The reversed correlation observed by Lattaud et al. (2016) could be explained by the BIT index representing proximity to the coast instead of sea level fluctuations.

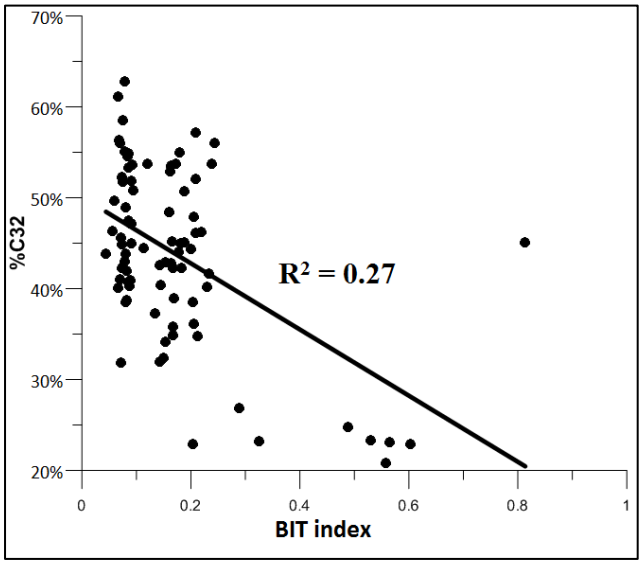

Figure 23. Cross plot showing the negative correlation between the %C32 and the BIT index (R^2 = 0.27).

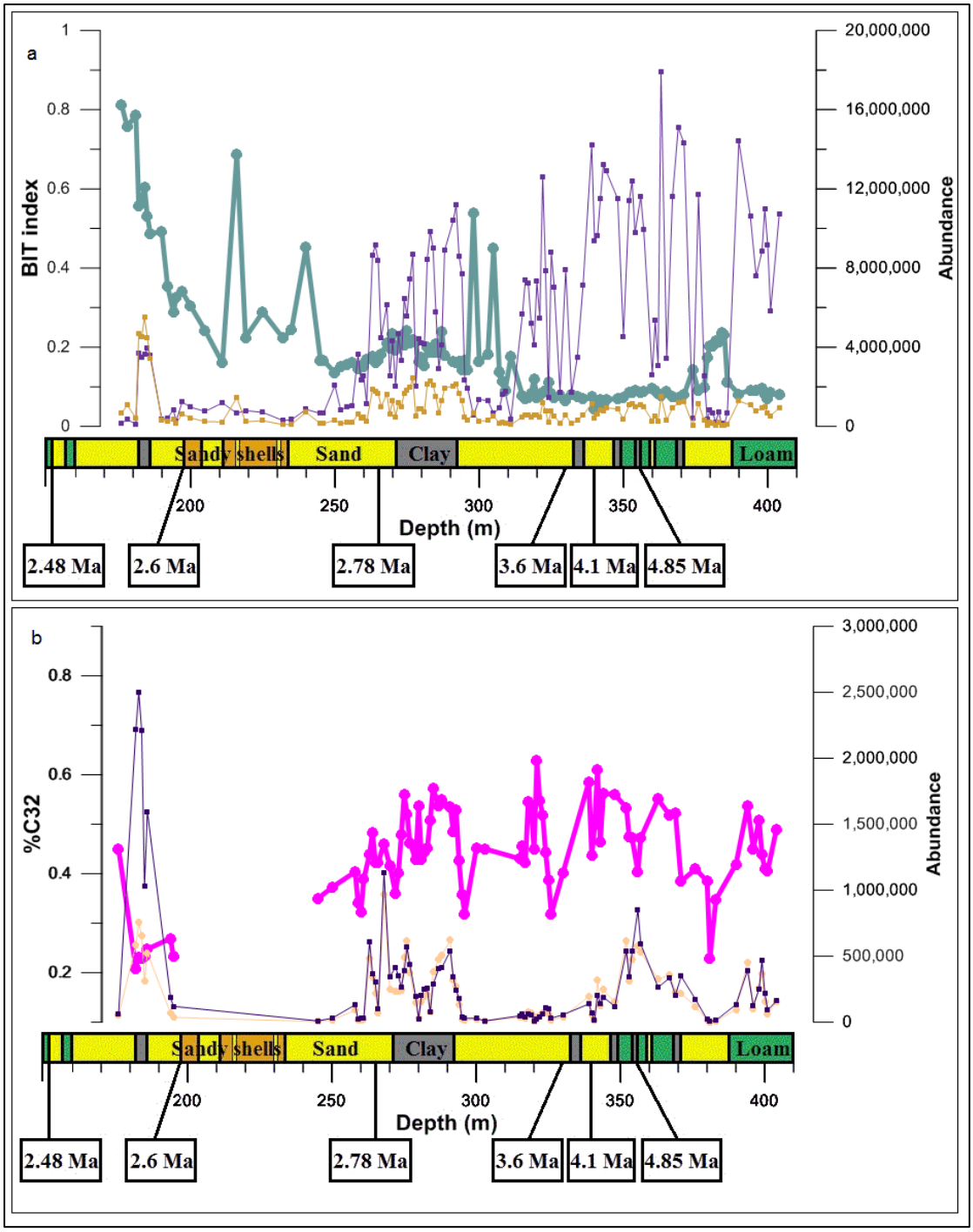

Figure 24. (a) The BIT index (green) and absolute values of crenarchaeol (purple) and the total of branched GDGTs (brown). (b) The %C32 (pink) and absolute values of the total of marine diols (blue) and the C_{32} 1,15-diol (orange).

Comparison of the records in Fig. 22 shows some interesting observations. Between 390 – 370 m, the MAT record shows cold temperatures. The $U^{K'}_{37}$ SST record shows low temperatures too, however, they are less pronounced than the MAT record. The BIT index is high, the %C32 is low, and the lithology consists mainly of sand. This period cannot be dated due to a lack of age points in that depth interval, however, it may be one of the earliest glaciation events of the Pliocene (De Schepper et al., 2014). The high BIT index indicates a low sea level, due to low temperatures (many continental ice sheets on earth). The %C32 indicates little river input, due to dry circumstances (much water captured in ice sheets). The main lithology is sand, which could be due to either proximal circumstances, or little river input. The SSTs do not show pronounced cooler circumstances when compared to the

terrestrial temperatures, indicating that SSTs are more influenced by ocean currents than by global climate. Between 210 – 190 m, similar features are seen in all proxies, which could also indicate glacial conditions. This period is interpreted as the MIS M2 glaciation event (~3.3 Ma; Dolan et al., 2015), based on the age points and comparison with the global benthic stack of the Pliocene (Lisiecki & Raymo, 2005). Between 296 – 258 m, the MAT record shows high temperatures. Using the same reasoning, this period is interpreted as the MPWP (3.3 – 3.0 Ma; Dowsett et al., 2010). This interval coincides with the high resolution part of the SST records, and with a thick (21 m) clay layer in the lithology. The SST records do not show the same features of the MPWP as the MAT record, which is remarkable (see section 4.4.1). Between 240 – 200 m, low temperatures are prevalent in the MAT record, the lithology consists of mainly sandy shells, and there are gaps in all three SST records. Cold global climate causes sea level fall, therefore moving the Hank site to a more proximal location. In this interval, marine biomarkers were not abundant enough to calculate SST, because of the shallow environment. Between 200 – 195 m is interpreted as being the last warm pulse of the Pliocene. At 195 m, the BIT index increases towards extreme high values and %C32 is decreasing. Based on the age tie points, this is interpreted as the start of the Pleistocene, right after the onset of NHG (sea level fall).

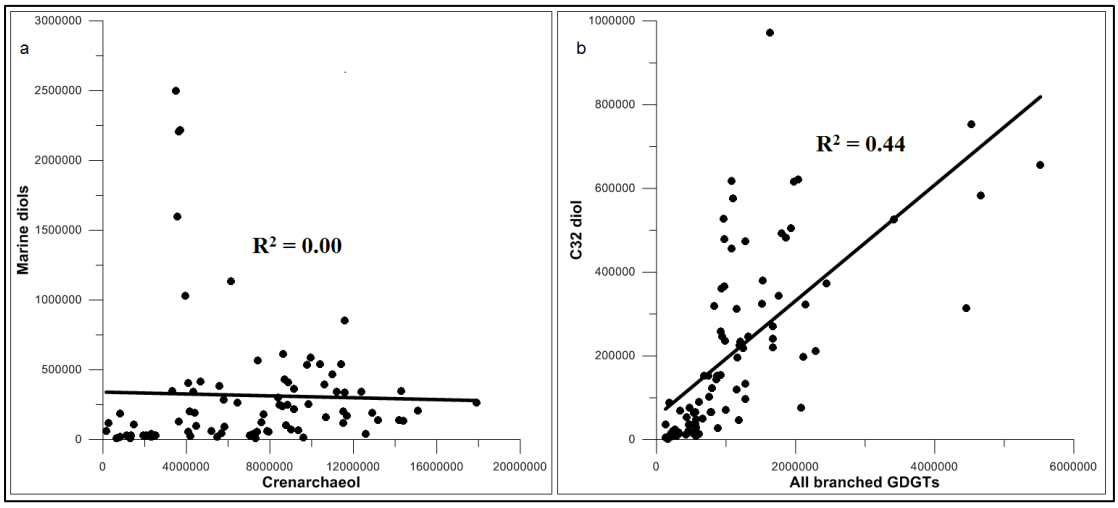

Figure 25. Cross plots showing the correlation between (a) the abundances of the total of marine diols and the marine GDGT crenarchaeol (R^2 = 0.00), and (b) the abundances of the C_{32} 1,15-diol and the total of all branched GDGTs (R^2 = 0.44).

Several conclusions can be drawn from the comparison of the marine climate, terrestrial climate, sea level fluctuations and river input. As SSTs show large fluctuations that are not visible in the terrestrial record, and global glaciation events visible in the MAT, BIT index and %C32 are not as pronounced in the SST records, it is assumed that SSTs are influenced by ocean currents. This confirms the theory of orbitally driven changes in the configuration of the NAC. The marine and terrestrial climate are decoupled because regional ocean currents appear to be the strongest control on SSTs, whereas global climate fluctuations control the terrestrial climate in this setting.

4.4.1. The Mid-Pliocene Warm Period

Proxy records of the MPWP (296 – 258 m; 3.3 – 3.0 Ma) interval, show several interesting features. Firstly, the MAT record shows high temperatures, however, the SST records show low and increasing temperatures (Fig. 22). All three SST records are higher in resolution in this interval compared to the other intervals (Fig. 6), indicating good preservation or biomarkers. Together with the lithology showing (pronounced clay layer), the depositional environment in this interval must have been different than the rest of the record. Perhaps this unique depositional environment could be the cause of the mismatch between the MAT and SST records. To investigate the depositional environment, the marine and terrestrial GDGTs of all Hank Core samples are plotted against each

other (Fig. 26). This approach gives an interesting insight about the depositional environment during the MPWP. The correlation between all branched GDGTs and crenarchaeol shows three distinct lines where correlation occurs (Fig. 26). The steepest line consists of Pleistocene samples. The depositional environment was really shallow during the Pleistocene, because of low sea level, therefore the abundance of marine GDGTs is relatively low compared to terrestrial GDGTs. The spreading of the samples over this line is likely caused by the hydrological climate, with dry (glacial) condition causing lower abundance and wet (interglacial) conditions causing higher abundance of (marine and terrestrial) GDGTs. The shallowest line consists of samples from the oldest part of the record (404 – 296 m). The sea level during the Pliocene was higher than in the Pleistocene, causing a deeper marine environment for the Hank Core and therefore relatively more marine GDGTs compared to terrestrial GDGTs. The middle line consists of only samples from the MPWP (296 -258 m) and raises a question why these samples plot on a different correlation line than all the other Pliocene samples. There are two hypotheses for these aberrant depositional circumstances.

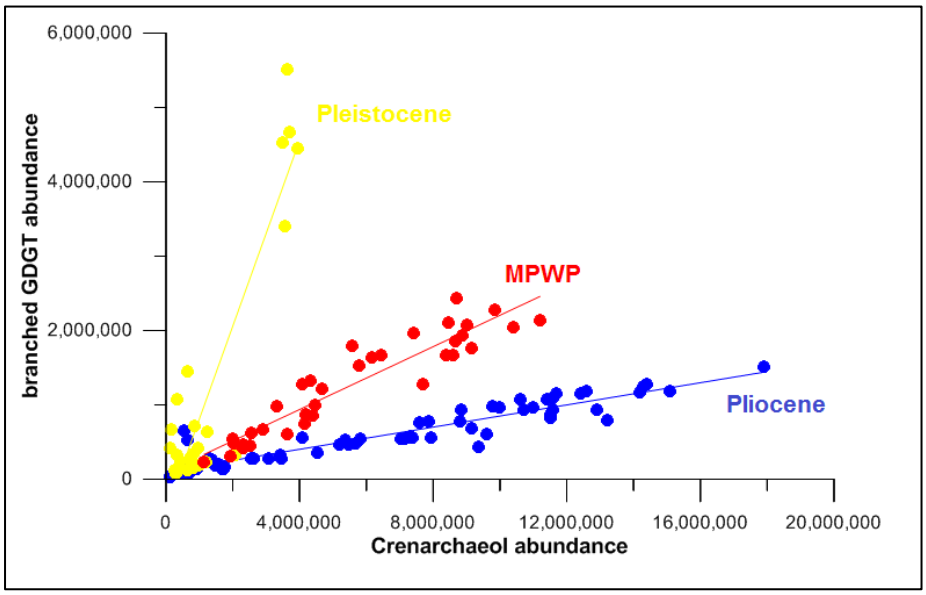

Figure 26. Cross plot showing the correlation between the abundances of the total of all branched GDGTs and crenarchaeol. The results plot on three lines, with Pleistocene samples plotting on the steepest line (yellow), MPWP samples plotting on the moderate line (red) and the other Pliocene samples plotting on the shallow line (blue).

The first hypothesis is that the aberrant ratio of branched GDGTs over crenarchaeol is caused by in situ production of branched GDGTs during the MPWP, which is possible on a specific depth in shallow seas according to Sinninghe Damsté (2016) and Fietz et al. (2012). A warmer global climate would have caused a rise in global sea level because of less continental ice caps on earth. In addition to that, the local sea level could be higher because of isostatic processes after the MIS M2 glacial preceding the MPWP. This isostasy could explain the local sea level to be higher than in the early Pliocene (global sea level is not expected to be higher in the MPWP than in the early Pliocene according to Miller et al. (2005) and Hilgen et al. (2012). The new distal location of the Hank Core leads to the formation of the pronounced clay layer (Fig. 22) and the high resolution SST results, due to less erosion and good preservation (Fig. 6). In particular, marine diols are in high abundance in this interval (Fig. 24b), confirming a deeper marine environment. However, the BIT index is higher and absolute values of crenarchaeol abundance are lower in the MPWP than in the early Pliocene (Fig. 24a), indicating a lower sea level or more proximal environment in the MPWP than in the early Pliocene, which contradicts this hypothesis.

The second hypothesis is that the aberrant ratio of branched GDGTs over crenarchaeol is caused by a different hydrological environment during the MPWP. Because of a warmer and thus wetter climate,

there would have been more river input, leading to higher concentrations of branched GDGTs. Warmer and wetter circumstances lead to more chemical weathering on land, causing the rivers to bring more clay into the marine environment, which explains the pronounced clay layer in the lithology. The higher resolution results of the SST records are due to a higher sedimentation rate because of more river input. The high abundance of the riverine C_{32} 1,15-diol (Fig. 24b) confirms this hypothesis. However, the lack of an increase in %C32 during the MPWP, contradicts this hypothesis.

A third hypothesis for this mismatch between MAT and SST records and the aberrant depositional environment is that different river systems may have been active during the MPWP. According to Kuhlmann et al. (2004), most late Pliocene North Sea sediments come from the precursor of the Rhine – Meuse fluvial system and the Eridanos fluvial system (coming from the Balthic area) was more active in the early Pliocene (Kuhlmann, 2004). The Eridanos fluvial system generally brought more fine sediments to the North Sea than the Rhine – Meuse sytem, and could perhaps cause the pronounced clay layer in the MPWP. However, according to Noorbergen et al. (2015), the Eridanos river system is directed towards northern seas like the Baltic Sea in warm periods, and the Rhine – Meuse system is believed to influence the North Sea in warm periods. Therefore, the river systems influencing the North Sea are probably the same in the MPWP as in the rest of the late Pliocene. Hence, this third hypothesis does not seem likely.

None of the hypotheses gives a satisfactory explanation for the mismatch between the MAT and SST record, which remains enigmatic. More information on the hydrological climate and the provenance of the sediment is needed to understand the mixed findings in the MPWP. In terms of likeliness, the second hypothesis seems to capture most of the explanation, because of the pronounced rise in BIT index during the MPWP (which contradicts the first hypothesis). A combination of higher sea level and more riverine input is also possible. The cold SSTs during the MPWP could be caused by different sea currents being active in the North Sea during the MPWP, or by different river input.

4.5. The alkenone pCO_2 proxy

To place the reconstructed sea surface temperatures in a global climate framework, I tried to reconstruct atmospheric CO_2 levels throughout the Pliocene. Measured values of $\delta^{13}C_{C37:2}$ range between -24.3 ‰ and -22.5 ‰. These correspond to Pliocene pCO_2 levels varying between 152 and 630 ppm (Fig. 27). The values seem to increase slightly during the Pliocene, and show one high outlier in the Pleistocene. This does not match with the temperature records of the Pliocene and early Pleistocene.

The pCO_2 alkenone proxy possesses large degrees of uncertainty, due to the many assumptions of environmental parameters needed. Cell physiology of haptophyte algae depends mainly on the amount of nutrients in surface waters, and as phosphate is often the limiting nutrient or serves as a proxy for other limiting nutrients, cell physiology is described by the concentration of soluble phosphate in the North Sea. Other environmental parameters, such as light intensity, are assumed to be constant. The largest uncertainty of the proxy is the phosphate concentration of the Pliocene North Sea. This is because it can vary significantly with distance to the coast, and the coastline of the Hank site most likely experienced large shifts during the Pliocene. Furthermore, variation in phosphate concentration has a large influence on the derived pCO_2 values (Bijl et al., 2010). In light of these uncertainties, pCO_2 values are calculated with errors bars representing pCO_2 with phosphate concentrations of 0.6 ± 0.2 µmol/L (Fig. 27). To have a more precise indication of pCO_2 values, a tool can be used to reconstruct phosphate concentrations. The remains of dinoflagellates (dinocysts), can be used for this, as they are known to be extremely sensitive to surface-water nutrient availability changes (Bijl et al., 2010). The ratio between peridinioid and gonyaulacoid dinocyst groups (the P/G

ratio) can be used to reconstruct changes in relative nutrient abundance (Sluijs et al., 2005). For further research to atmospheric pCO_2 concentrations of the Pliocene in the North Sea, I would recommend to use this P/G ratio to indicate phosphate concentrations. For now, I can conclude that I have a rough indication of how atmospheric pCO_2 values were during the Pliocene, but many uncertainties remain and the pCO_2 values remain very uncertain.

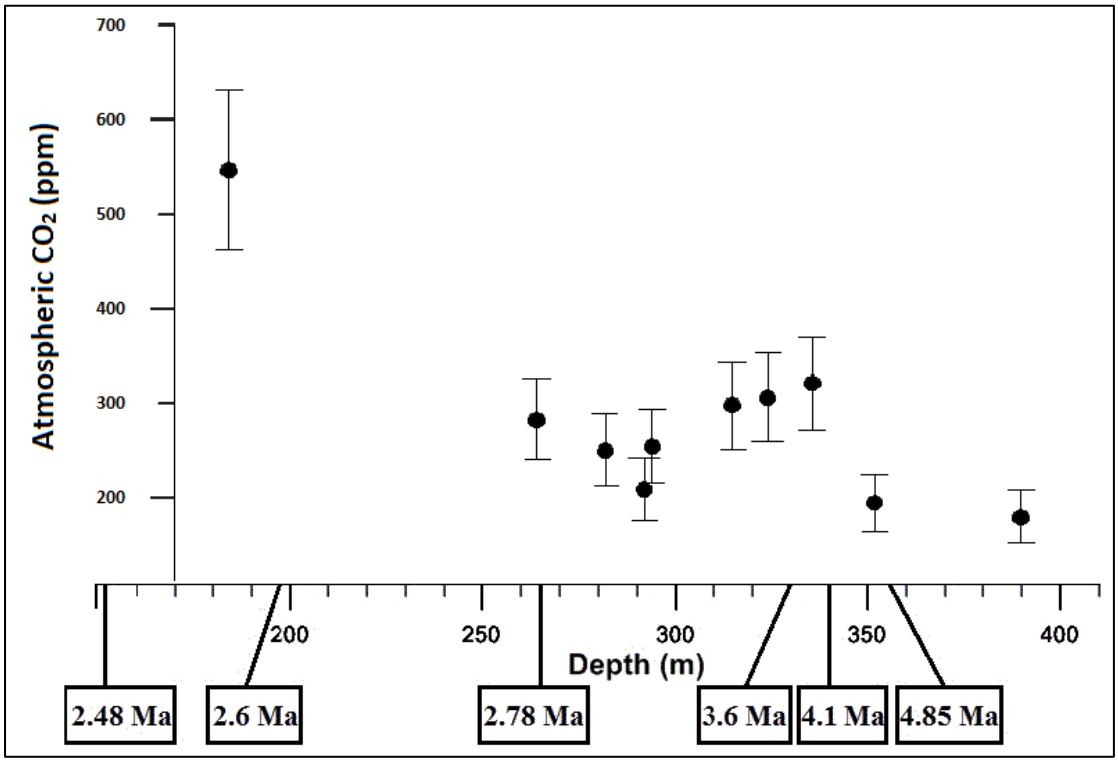

Figure 27. Atmospheric CO_2 concentrations of the Pliocene and early Pleistocene with error bars for Phosphate concentrations of 0.6 ± 0.2.

5. Conclusions

In this thesis, marine biomarkers were measured to compare organic proxy SST records during the Pliocene. The SST proxy comparison shows that the $U^{K'}_{37}$ and LDI proxies respond to the same driver, which is sea surface temperature, but to different extents. The differences in absolute SST values of the two proxies are caused by different production seasons of the proxy-biomarkers. Due to the relatively shallow water column and latitudinal position, the North Sea experiences large seasonal temperature differences, so the different production seasons result in large variations in reconstructed SSTs. The TEX_{86}^{H} proxy mismatches the other two SST proxies and is therefore not reliable here. The large fluctuations in SSTs confirm that the Atlantic system was unstable during the Pliocene. The fluctuations are caused by changes in the configuration of the North Atlantic current and Arctic front, driven by orbitally changes in solar insolation. The terrestrial and marine climate are decoupled from each other, as the marine climate is mainly influenced by regional ocean currents, and the terrestrial climate by global climate fluctuations.

Acknowledgements

I would like to acknowledge Peter Bijl for help with pCO_2 calculations and understanding of the proxy, Anita van Leeuwen, Dominika Kasjaniuk, Arnold van Dijk and Anchelique Mets for help in the lab, Stefan Schouten for help with analysis of diols, Frits Hilgen for help with spectral analysis and interpretation of cyclicities and Dirk Munsterman for the samples and the age model.

References

Baranova, O. (2015). World ocean atlas 2005.

Bartoli, G., Sarnthein, M., Weinelt, M., Erlenkeuser, H., Garbe-Schönberg, D., & Lea, D. W. (2005). Final closure of Panama and the onset of northern hemisphere glaciation. Earth and Planetary Science Letters, 237(1), 33-44.

Bijl, P. K., Houben, A. J., Schouten, S., Bohaty, S. M., Sluijs, A., Reichart, G. J., ... & Brinkhuis, H. (2010). Transient Middle Eocene atmospheric CO2 and temperature variations. Science, 330(6005), 819-821.

Chapman, M. R., Shackleton, N. J., Zhao, M., & Eglinton, G. (1996). Faunal and alkenone reconstructions of subtropical North Atlantic surface hydrography and paleotemperature over the last 28 kyr. Paleoceanography, 11(3), 343-357.

Damsté, J. S. S. (2016). Spatial heterogeneity of sources of branched tetraethers in shelf systems: The geochemistry of tetraethers in the Berau River delta (Kalimantan, Indonesia). Geochimica et Cosmochimica Acta, 186, 13-31.

De Schepper, S., Groeneveld, J., Naafs, B. D. A., Van Renterghem, C., Hennissen, J., Head, M. J., ... & Fabian, K. (2013). Northern hemisphere glaciation during the globally warm early late Pliocene. PloS one, 8(12), e81508.

De Schepper, S., Gibbard, P. L., Salzmann, U., & Ehlers, J. (2014). A global synthesis of the marine and terrestrial evidence for glaciation during the Pliocene Epoch. Earth-Science Reviews, 135, 83-102.

De Schepper, S., Schreck, M., Beck, K. M., Matthiessen, J., Fahl, K., & Mangerud, G. (2015). Early Pliocene onset of modern Nordic Seas circulation related to ocean gateway changes. Nature communications, 6.

Dearing Crampton Flood, E., Peterse, F., Munsterman, D., & Sinninghe Damste, J. (in prep.). A terrestrial Pliocene-Pleistocene temperature record from North-Western Europe.

Dolan, A. M., Haywood, A. M., Hunter, S. J., Tindall, J. C., Dowsett, H. J., Hill, D. J., & Pickering, S. J. (2015). Modelling the enigmatic Late Pliocene Glacial Event—Marine Isotope Stage M2. Global and Planetary Change, 128, 47-60.

Dowsett, H. J. (2007). The PRISM palaeoclimate reconstruction and Pliocene sea-surface temperature. Deep-time perspectives on climate change: marrying the signal from computer models and biological proxies, 459-480.

Dowsett, H. J., Chandler, M. A., & Robinson, M. M. (2009). Surface temperatures of the Mid-Pliocene North Atlantic Ocean: implications for future climate. Philosophical Transactions of the Royal Society of London A: Mathematical, Physical and Engineering Sciences, 367(1886), 69-84.

Dowsett, H., Robinson, M., Haywood, A. M., Salzmann, U., Hill, D., Sohl, L. E., ... & Stoll, D. K. (2010). The PRISM3D paleoenvironmental reconstruction. Stratigraphy, 7(2-3), 123-139.

Dowsett, H. J., Robinson, M. M., Haywood, A. M., Hill, D. J., Dolan, A. M., Stoll, D. K., ... & Otto-Bliesner, B. L. (2012). Assessing confidence in Pliocene sea surface temperatures to evaluate predictive models. Nature Climate Change, 2(5), 365-371.

Fietz, S., Huguet, C., Bendle, J., Escala, M., Gallacher, C., Herfort, L., ... & Prahl, F. G. (2012). Co-variation of crenarchaeol and branched GDGTs in globally-distributed marine and freshwater sedimentary archives. Global and Planetary Change, 92, 275-285.

Gong, C., & Hollander, D. J. (1999). Evidence for differential degradation of alkenones under contrasting bottom water oxygen conditions: Implication for paleotemperature reconstruction. Geochimica et Cosmochimica Acta, 63(3), 405-411.

Grenander, U. (1959). Probability and statistics: the Harald Cramér volume, 434.

Hardee, M. L., & Thunell, R. C. (2007). Alkenone Production and UK'37 Temperature Estimates: A Time-Series Study in the Santa Barbara Basin, California. In AGU Fall Meeting Abstracts (Vol. 1, p. 1257).

Haywood, A. M., Dowsett, H. J., Valdes, P. J., Lunt, D. J., Francis, J. E., & Sellwood, B. W. (2009). Introduction. Pliocene climate, processes and problems. Philosophical Transactions of the Royal Society of London A: Mathematical, Physical and Engineering Sciences, 367(1886), 3-17.

Herfort, L., Schouten, S., Boon, J. P., & Damsté, J. S. S. (2006). Application of the TEX 86 temperature proxy to the southern North Sea. Organic Geochemistry, 37(12), 1715-1726.

Hilgen, F. J., Lourens, L. J., & Van Dam, J. A. (2012). The neogene period.

Hoefs, M. J., Versteegh, G. J., Rijpstra, W. I. C., Leeuw, J. W., & Damsté, J. S. S. (1998). Postdepositional oxic degradation of alkenones: Implications for the measurement of palaeo sea surface temperatures. Paleoceanography, 13(1), 42-49.

Hopmans, E. C., Weijers, J. W., Schefuß, E., Herfort, L., Damsté, J. S. S., & Schouten, S. (2004). A novel proxy for terrestrial organic matter in sediments based on branched and isoprenoid tetraether lipids. Earth and Planetary Science Letters, 224(1), 107-116.

Huuse, M., Lykke-Andersen, H., Michelsen, O. (2001). Cenozoic evolution of the eastern North Sea Basin – new evidence from high-resolution and conventional seismic data. Marine Geology, 177, 243-269.

Huuse, M. and Clausen, O.R. (2001). Morphology and origin of major Cenozoic sequence boundaries in the eastern North Sea Basin: top Eocene, near-top Oligocene and the mid-Miocene unconformity. Basin Research, 13, 17-41.

Jia, G., Rao, Z., Zhang, J., Li, Z., & Chen, F. (2013). Tetraether biomarker records from a loess-paleosol sequence in the western Chinese Loess Plateau. Frontiers in microbiology, 4.

Kim, J. H., Schouten, S., Hopmans, E. C., Donner, B., & Damsté, J. S. S. (2008). Global sediment core-top calibration of the TEX 86 paleothermometer in the ocean. Geochimica et Cosmochimica Acta, 72(4), 1154-1173.

Kim, J. H., Huguet, C., Zonneveld, K. A., Versteegh, G. J., Roeder, W., Damsté, J. S. S., & Schouten, S. (2009). An experimental field study to test the stability of lipids used for the TEX 86 and palaeothermometers. Geochimica et Cosmochimica Acta, 73(10), 2888-2898.

Kim, J. H., Van der Meer, J., Schouten, S., Helmke, P., Willmott, V., Sangiorgi, F., ... & Damsté, J. S. S. (2010). New indices and calibrations derived from the distribution of crenarchaeal isoprenoid tetraether lipids: Implications for past sea surface temperature reconstructions. Geochimica et Cosmochimica Acta, 74(16), 4639-4654.

Kuhlmann, G. (2004). High resolution stratigraphy and paleoenvironmental changes in the southern North Sea during the Neogene: an integrated study of Late Cenozoic marine deposits from the northern part of the Dutch offshore area. UU Dept. of Earth Sciences.

Kuhlmann, G., de Boer, P. L., Pedersen, R. B., & Wong, T. E. (2004). Provenance of Pliocene sediments and paleoenvironmental changes in the southern North Sea region using Samarium–Neodymium (Sm/Nd) provenance ages and clay mineralogy. Sedimentary Geology, 171(1), 205-226.

Kuhlmann, G., Langereis, C. G., Munsterman, D., Leeuwen, R. J. V., Verreussel, R., Meulenkamp, J. E., & Wong, T. E. (2006). Integrated chronostratigraphy of the Pliocene-Pleistocene interval and its relation to the regional stratigraphical stages in the southern North Sea region. Netherlands Journal of Geosciences/Geologie en Mijnbouw, 85(1), 19-35.

Laskar, J. (1990). The chaotic motion of the solar system: a numerical estimate of the size of the chaotic zones. Icarus, 88(2), 266-291.

Lattaud, J., De Jonge, C., Kim, J. H., Zell, C., Damsté, J. S., & Sschouten, S. The C32 Alkane-1, 15-Diol as a Tracer for Riverine Input in Coastal Seas. Presented at the Goldschmidt Conference, 2016.

Lawrence, K. T., Herbert, T. D., Brown, C. M., Raymo, M. E., & Haywood, A. M. (2009). High-amplitude variations in North Atlantic sea surface temperature during the early Pliocene warm period. Paleoceanography, 24(2).

Lee, K. E., Kim, J. H., Wilke, I., Helmke, P., & Schouten, S. (2008). A study of the alkenone, TEX86, and planktonic foraminifera in the Benguela Upwelling System: implications for past sea surface temperature estimates. Geochemistry, Geophysics, Geosystems, 9(10).

Lisiecki, L. E., & Raymo, M. E. (2005). A Pliocene-Pleistocene stack of 57 globally distributed benthic δ18O records. Paleoceanography, 20(1).

Londeix, L., Benzakour, M., Suc, J. P., & Turon, J. L. (2007). Messinian palaeoenvironments and hydrology in Sicily (Italy): the dinoflagellate cyst record. Geobios, 40(3), 233-250.

Louwye, S., HEAD, M. J., & DE SCHEPPER, S. (2004). Dinoflagellate cyst stratigraphy and palaeoecology of the Pliocene in northern Belgium, southern North Sea Basin. Geological Magazine, 141(03), 353-378.

Martínez-Botí, M. A., Foster, G. L., Chalk, T. B., Rohling, E. J., Sexton, P. F., Lunt, D. J., ... & Schmidt, D. N. (2015). Plio-Pleistocene climate sensitivity evaluated using high-resolution CO2 records. Nature, 518(7537), 49-54.

Meijer, T., Cleveringa, P., Munsterman, D. K., & Verreussel, R. M. C. H. (2006). The Early Pleistocene Praetiglian and Ludhamian pollen stages in the North Sea Basin and their relationship to the marine isotope record. Journal of Quaternary Science, 21(3), 307-310.

Miller, K. G., Kominz, M. A., Browning, J. V., Wright, J. D., Mountain, G. S., Katz, M. E., ... & Pekar, S. F. (2005). The Phanerozoic record of global sea-level change. Science, 310(5752), 1293-1298.

Mudie, P. J. (1987). Palynology and dinoflagellate biostratigraphy of deep-sea drilling project Leg-94, Site-607 and Site-611, North Atlantic Ocean. Initial Reports of the Deep Sea Drilling Project, 94, 785.

Müller, P. J., Kirst, G., Ruhland, G., Von Storch, I., & Rosell-Melé, A. (1998). Calibration of the alkenone paleotemperature index U 37 K' based on core-tops from the eastern South Atlantic and the global ocean (60 N-60 S). Geochimica et Cosmochimica Acta, 62(10), 1757-1772.

Naafs, B. D. A., Stein, R., Hefter, J., Khélifi, N., De Schepper, S., & Haug, G. H. (2010). Late Pliocene changes in the North Atlantic current. Earth and Planetary Science Letters, 298(3), 434-442.

Naafs, B. D. A., Hefter, J., & Stein, R. (2012). Application of the long chain diol index (LDI) paleothermometer to the early Pleistocene (MIS 96). Organic geochemistry, 49, 83-85.

Noorbergen, L. J., Lourens, L. J., Munsterman, D. K., & Verreussel, R. M. C. H. (2015). Stable isotope stratigraphy of the early Quaternary of borehole Noordwijk, southern North Sea. Quaternary International, 386, 148-157.

Pagani, M. (2002). The alkenone-CO2 proxy and ancient atmospheric carbon dioxide. Philosophical Transactions of the Royal Society of London A: Mathematical, Physical and Engineering Sciences, 360(1793), 609-632.

Pagani, M., Zachos, J. C., Freeman, K. H., Tipple, B., & Bohaty, S. (2005). Marked decline in atmospheric carbon dioxide concentrations during the Paleogene. Science, 309(5734), 600-603.

Pagani, M., Liu, Z., LaRiviere, J., & Ravelo, A. C. (2010). High Earth-system climate sensitivity determined from Pliocene carbon dioxide concentrations. Nature Geoscience, 3(1), 27-30.

Paillard, D., Labeyrie, L., & Yiou, P. (1996). Macintosh program performs time-series analysis. Eos, Transactions American Geophysical Union, 77(39), 379-379.

Pitcher, A., Wuchter, C., Siedenberg, K., Schouten, S., & Sinninghe Damsté, J. S. (2011). Crenarchaeol tracks winter blooms of ammonia-oxidizing Thaumarchaeota in the coastal North Sea. Limnology and Oceanography, 56(6), 2308-2318.

Plancq, J., Grossi, V., Pittet, B., Huguet, C., Rosell-Melé, A., & Mattioli, E. (2015). Multi-proxy constraints on sapropel formation during the late Pliocene of central Mediterranean (southwest Sicily). Earth and Planetary Science Letters, 420, 30-44.

Popp, B. N., Laws, E. A., Bidigare, R. R., Dore, J. E., Hanson, K. L., & Wakeham, S. G. (1998). Effect of phytoplankton cell geometry on carbon isotopic fractionation. Geochimica et Cosmochimica Acta, 62(1), 69-77.

Prahl, F. G., & Wakeham, S. G. (1987). Calibration of unsaturation patterns in long-chain ketone compositions for palaeotemperature assessment. Nature 330, 367 – 369.

Prahl, F. G., Sparrow, M. A., & Wolfe, G. V. (2003). Physiological impacts on alkenone paleothermometry. Paleoceanography, 18(2).

Rampen, S. W., Willmott, V., Kim, J. H., Uliana, E., Mollenhauer, G., Schefuß, E., ... & Schouten, S. (2012). Long chain 1, 13-and 1, 15-diols as a potential proxy for palaeotemperature reconstruction. Geochimica et Cosmochimica Acta, 84, 204-216.

Rodrigo-Gámiz, M., Martínez-Ruiz, F., Rampen, S. W., Schouten, S., & Sinninghe Damsté, J. S. (2014). Sea surface temperature variations in the western Mediterranean Sea over the last 20 kyr: A dual-organic proxy (UK' 37 and LDI) approach. Paleoceanography, 29(2), 87-98.

Rodrigo-Gámiz, M., Rampen, W., Haas, H. D., Baas, M., Schouten, S., & Sinninghe Damsté, J. S. (2015). Constraints on the applicability of the organic temperature proxies UK'37, TEX86 and LDI in the subpolar region around Iceland. Biogeosciences, 12, 6573-2015.

Rommerskirchen, F., Condon, T., Mollenhauer, G., Dupont, L., & Schefuss, E. (2011). Miocene to Pliocene development of surface and subsurface temperatures in the Benguela Current system. Paleoceanography, 26(3).

Rontani, J. F., Volkman, J. K., Prahl, F. G., & Wakeham, S. G. (2013). Biotic and abiotic degradation of alkenones and implications for paleoproxy applications: A review. Organic geochemistry, 59, 95-113.

Schouten, S., Hopmans, E. C., Schefuß, E., & Damste, J. S. S. (2002). Distributional variations in marine crenarchaeotal membrane lipids: a new tool for reconstructing ancient sea water temperatures?. Earth and Planetary Science Letters, 204(1), 265-274.

Schouten, S., Hopmans, E. C., & Damsté, J. S. S. (2013). The organic geochemistry of glycerol dialkyl glycerol tetraether lipids: a review. Organic geochemistry, 54, 19-61.

Sluijs, A., Pross, J., & Brinkhuis, H. (2005). From greenhouse to icehouse; organic-walled dinoflagellate cysts as paleoenvironmental indicators in the Paleogene. Earth-Science Reviews, 68(3), 281-315.

Stiltz, H. L. (Ed.). (1961). Aerospace telemetry (Vol. 1). Prentice Hall.

Versteegh, G. J. M., Bosch, H. J., & De Leeuw, J. W. (1997). Potential palaeoenvironmental information of C 24 to C 36 mid-chain diols, keto-ols and mid-chain hydroxy fatty acids; a critical review. Organic Geochemistry, 27(1), 1-13.

Villanueva, L., Besseling, M., Rodrigo-Gámiz, M., Rampen, S. W., Verschuren, D., & Damsté, J. S. S. (2014). Potential biological sources of long chain alkyl diols in a lacustrine system. Organic Geochemistry, 68, 27-30.

Weiss, R. (1974). Carbon dioxide in water and seawater: the solubility of a non-ideal gas. Marine chemistry, 2(3), 203-215.

Ziegler. (1990). Geological atlas of Western and Central Europe. 3nd edition, Shell International Petroleum Maatschappij B.V. 239 pp